

Partial cross mapping eliminates indirect causal influences

Siyang Leng ^{1,2,3}, Huanfei Ma ⁴, Jürgen Kurths^{5,6}, Ying-Cheng Lai ⁷, Wei Lin ^{1,2,8}✉, Kazuyuki Aihara ^{3,9}✉ & Luonan Chen ^{10,11,12,13}✉

Causality detection likely misidentifies indirect causations as direct ones, due to the effect of causation transitivity. Although several methods in traditional frameworks have been proposed to avoid such misinterpretations, there still is a lack of feasible methods for identifying direct causations from indirect ones in the challenging situation where the variables of the underlying dynamical system are non-separable and weakly or moderately interacting. Here, we solve this problem by developing a data-based, model-independent method of partial cross mapping based on an articulated integration of three tools from nonlinear dynamics and statistics: phase-space reconstruction, mutual cross mapping, and partial correlation. We demonstrate our method by using data from different representative models and real-world systems. As direct causations are keys to the fundamental underpinnings of a variety of complex dynamics, we anticipate our method to be indispensable in unlocking and deciphering the inner mechanisms of real systems in diverse disciplines from data.

¹School of Mathematical Sciences, SCMS, SCAM, and LMNS, Fudan University, 200433 Shanghai, China. ²Center for Computational Systems Biology of ISTBI, LCNBI, and Research Institute of Intelligent Complex Systems, Fudan University, 200433 Shanghai, China. ³Institute of Industrial Science, University of Tokyo, Tokyo 153-8505, Japan. ⁴School of Mathematical Sciences, Soochow University, 215006 Suzhou, China. ⁵Potsdam Institute for Climate Impact Research, Potsdam 14412, Germany. ⁶Saratov State University, Saratov 410012, Russia. ⁷School of Electrical, Computer, and Energy Engineering, Arizona State University, Tempe, AZ 85287-5706, USA. ⁸State Key Laboratory of Medical Neurobiology, and MOE Frontiers Center for Brain Science, Institutes of Brain Science, Fudan University, 200032 Shanghai, China. ⁹International Research Center for Neurointelligence (IRCIN), University of Tokyo, Tokyo 113-0033, Japan. ¹⁰Center for Excellence in Molecular Cell Science, Institute of Biochemistry and Cell Biology, Chinese Academy of Sciences, 200031 Shanghai, China. ¹¹Center for Excellence in Animal Evolution and Genetics, Chinese Academy of Sciences, 650223 Kunming, China. ¹²Institute of Brain-Intelligence Technology, Zhangjiang Laboratory, 201210 Shanghai, China. ¹³Key Laboratory of Systems Biology, Hangzhou Institute for Advanced Study, University of Chinese Academy of Sciences, Chinese Academy of Sciences, 310024 Hangzhou, China. ✉email: wlin@fudan.edu.cn; aihara@sat.t.u-tokyo.ac.jp; lnchen@sibs.ac.cn

Causal interactions are fundamental underpinnings in natural and engineering systems, as well as in social, economical, and political systems. Here system details are typically not known, but only time series are available. Correctly identifying causal relations among the dynamical variables generating the time series provides a window through which the inner dynamics of the target system may be probed into, and a number of previous methods were developed, such as those based on the celebrated Granger causality^{1–5}, the entropy^{6–11}, the dynamical Bayesian inference^{12–15}, and the mutual cross mapping (MCM)^{16–21}, with applications to real-world systems^{5,7,22–31}. If the system contains two independent variables only, the causal relation between them is straightforwardly direct. However, for a complex system with a large number of interacting nodes connected with each other in a networked fashion, two kinds of causation can arise: direct and indirect. Especially, if there is a direct link between two nodes, the detected causal relation between them can contain a direct component and an indirect one through other nodes in the network as a result of the generic phenomenon of causation transitivity (see Fig. 1). Even for two nodes that are not directly connected, a causal relation may be detected, but it must be indirect. To eliminate indirect causal influences so as to ascertain direct causal links is of paramount importance, as the latter constitutes the base for modeling, predicting, and controlling the system. There were previous studies of significant advance in detecting direct causal links to reconstruct the underlying true causal network based on the concept of partial transfer entropy or its linear Gaussian version, the conditional Granger causality, which resulted in many successful data mining in related fields^{32–38}. Combining these methods with graphical models, recent studies further provided a visible and comprehensive description of causal relations among interested variables^{36,38,39}. However, mathematically, all these methods are not applicable directly in situations where the relevant dynamical variables are non-separable so that the information from any variables cannot be separated easily in a prediction framework (see “Methods” for the rigorous concept of

non-separability). In real-world nonlinear systems, the non-separability is ubiquitously present among systems variables¹⁷. To our knowledge, the problem of ascertaining direct causation by removing indirect causal influences for general complex dynamical systems has not been fully studied and remained outstanding.

In this paper, we develop a data-based, model-free method of partial cross mapping (PCM) to eliminate indirect causal influences in situations where non-separability is allowed to be present. The central idea is to integrate three basic data analysis methods from nonlinear dynamics and statistics: classic phase-space reconstruction, MCM, and partial correlation, to detect direct causal links for complex and nonlinear networked systems. The method is validated using various benchmark systems. Its applications to real-world systems lead to new insights into their dynamical underpinnings. The method provides a solution to the long-standing, crucial problem with existing causality detection methods: misidentifying indirect causal influences as direct ones. Because of its unprecedented ability to eliminate indirect causation, this method can be a powerful tool to understand and model complex dynamical systems.

Results

Direct and indirect causal links. To illustrate the difference between direct and indirect causal links, we first consider a toy system of three variables with different interaction structures. If only two variables interact in one direction and the third one is isolated (Fig. 1a), then the previous methods can be effective for identifying the direct causal link^{16–21}. However, when the three variables constitute a unidirectional causal chain (Fig. 1b), applying any of the previous methods to the time series from a pair of variables would detect a false direct link between the two non-neighboring variables X and Y in Fig. 1b (see “Methods” for a false link aroused by the transitivity). When the three variables constitute a causal loop (Fig. 1c), every two neighboring variables may have an indirect causal link in addition to the direct one in the opposite direction. In this case, previous methods would falsely identify any actual indirect link as a direct one. In addition to the above three representative interaction structures for the three variables, all the other possible modes have been introduced thoroughly and investigated systematically in Supplementary Note 1. Moreover, with more observable variables, the likelihood that indirect causal links are incorrectly regarded as direct ones will substantially increase (Fig. 1d).

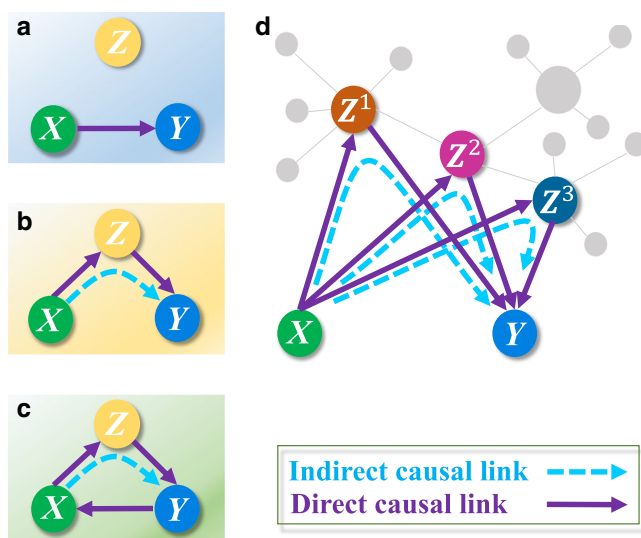


Fig. 1 Direct versus indirect causal links. **a** There is directional interaction between variables X and Y , but Z is an independent variable. **b** The variables X , Y , and Z constitute a one-directional causal chain with an indirect causal link from X to Y . **c** The variables constitute a causal loop, where every two neighboring variables have, in two opposite directions, a direct and an indirect causal link, respectively. **d** For a network with many interacting variables, more indirect causal links would be falsely identified as direct causal links.

Partial cross mapping. To overcome this problem, we propose the PCM method. The key idea is to examine the consensus between one time series and its cross map prediction from the other with conditioning on the part that is transferred from the third variable. For the convenience of describing our method clearly, we consider the simple case of three variables (X , Y , and Z) causally interacting with each other in a unidirectional chain (Fig. 2a). Let $X = \{x_t\}_{t=1}^L$, $Y = \{y_t\}_{t=1}^L$, and $Z = \{z_t\}_{t=1}^L$ be the corresponding time series of length L . Using Takens–Mañé’s delay-coordinate embedding^{40,41}, we obtain three shadow manifolds: $M_X = \{\mathbf{x}_t\}_{t=r}^L$, $M_Y = \{\mathbf{y}_t\}_{t=r}^L$, and $M_Z = \{\mathbf{z}_t\}_{t=r}^L$ with the vectors

$$\mathbf{x}_t = (x_t, x_{t-\tau_x}, \dots, x_{t-(E_x-1)\tau_x}),$$

$$\mathbf{y}_t = (y_t, y_{t-\tau_y}, \dots, y_{t-(E_y-1)\tau_y}),$$

$$\mathbf{z}_t = (z_t, z_{t-\tau_z}, \dots, z_{t-(E_z-1)\tau_z}),$$

where E_x , E_y , and E_z are the respective embedding dimensions, τ_x , τ_y , and τ_z are the time lags, and $r = \max_{\xi=x,y,z} \{1 + (E_\xi - 1)\tau_\xi\}$.

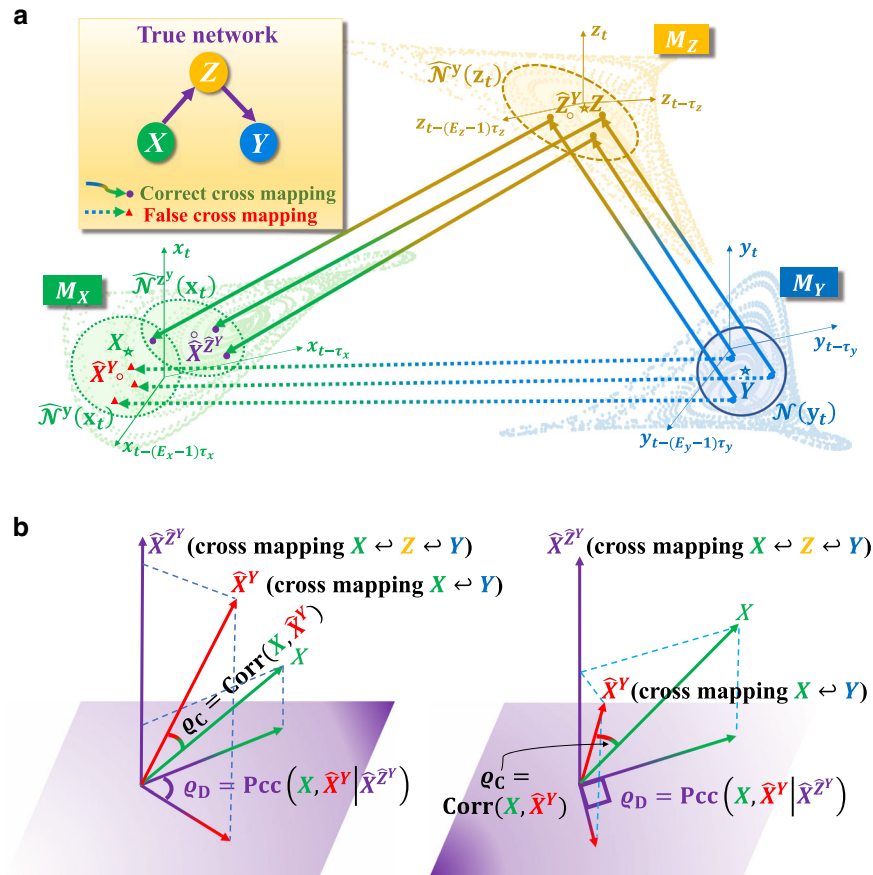


Fig. 2 Basic principles of the PCM framework. **a** For the illustrative setting of three variables interacting in a unidirectional causal chain, the MCM method maps $\mathcal{N}(y_t)$ to the left circled region $\hat{N}^Y(x_t)$ in M_X , where the estimated \hat{X}^Y is close to the true X , denoting full causal information from X to Y and leading to erroneous identification of the indirect causal link as the direct link. **b** For our proposed PCM method, partial correlation coefficient between X and \hat{X}^Y is calculated by conditioning on the information about \hat{X}^Z , which is mapped from $\mathcal{N}(y_t)$ through M_Z and then to the right circled region $\hat{N}^Z(x_t)$ in M_X in **a**, denoting indirect information flow. Geometrically, q_C corresponds to the cosine of the angle between X and \hat{X}^Y in the entire space, while q_D is the projection of q_C onto the subspace orthogonal to \hat{X}^Z . Because $q_C \geq q_D$, the example in **a** corresponds to the sketch on the right side of **b**, where the projection is close to the right angle, leading to a near-zero value of q_D .

These parameters of embedding dimensions and time lags can be computationally determined by the method of false nearest neighbor (FNN) and delayed mutual information (DMI), respectively. More advanced techniques can also be utilized^{20,42}. In general, for any pair of variables ξ and $\eta \in \{x, y, z\}$, we set $\hat{N}^\xi(\eta_t) = \{\eta_{t'} | \xi_{t'} \in \mathcal{N}(\xi_t)\}$, where $\mathcal{N}(\xi_t)$ is a set containing a fixed number (usually taken as $E_\xi + 1$, which is the minimum number of points needed for a bounded simplex in an E_ξ -dimensional space⁴³) of nearest neighboring points of ξ_t in the corresponding shadow manifold. For $\xi = \eta$, $\hat{N}^\xi(\eta_t)$ becomes $\mathcal{N}(\eta_t)$. For $\xi \neq \eta$, $\hat{N}^\xi(\eta_t)$ becomes a cross mapping neighborhood from $\mathcal{N}(\xi_t)$ (for an illustrative example, see the horizontal arrows from M_Y to M_X in Fig. 2a). The dependence from $\mathcal{N}(\eta_t)$ to $\hat{N}^\xi(\eta_t)$ characterizes the causal influence from the variable producing η_t to the variable producing ξ_t . Previously developed heuristic measures for quantifying such dependence and causal influence^{16–18,20,21} constitute the MCM framework. We exploit the correlation coefficient¹⁷ between η_t and $\hat{\eta}_t^\xi = \mathbb{E}[\hat{N}^\xi(\eta_t)]$, where $\hat{\eta}_t^\xi$ is the mapping from ξ_t and $\mathbb{E}[\cdot]$ is an operation taking appropriately weighted average over all the points in a given set.

Specifically, if the correlation coefficient $q_C = |\text{Corr}(x_t, \hat{x}_t^y)|$ is larger than an empirical threshold T , the MCM method will stipulate that there is a causal influence from X to Y . MCM complements the field of causality analysis in pairwise non-separable dynamical systems. However, due to causation transitivity, the causal link detected by MCM can be either direct or indirect, as illustrated in Fig. 2a. Additionally, since causation manifests its influence in a certain time delay, we search for an optimal time delay that maximizes the causation (i.e., the obtained correlation coefficient q_C) between a translated Y and X (see “Methods” for a detailed description)²⁰.

Heuristically, q_C , as defined above, represents the cosine of the angle between X and \hat{X}^Y in the entire space, as shown in Fig. 2b. In order to distinguish the existence of the causation transitivity, we consider the projection of q_C onto the information space orthogonal to the indirect information that is induced by the causation transitivity. To this end, we formulate our PCM framework (see “Methods” and Supplementary Fig. 1 for detailed formulations and practical instructions). First, for a time series pair Z and translated $Y_{\tau_i} = \{y_{t+\tau_i}\}$ with possible time delay candidates $\tau_i (i = 1, 2, \dots, m)$, we apply the conventional MCM method to determine the optimal time delay $\tau_i = \tau_{i^*}$, which

maximizes the correlation coefficient $\text{Corr}(Z, \hat{Z}^{Y_{\tau_1}})$. Correspondingly, the obtained mapping $\hat{Z}^{Y_{\tau_1}}$ from Y_{τ_1} is denoted by \hat{Z}^Y for simplicity. The next step is to repeat the procedure to the time series pair X and the translated $\hat{Z}^{Y_{\tau_1}}$ so as to obtain the optimal time delay τ_2 , as well as the mapping $\hat{X}^{\hat{Z}^{Y_{\tau_2}}}$ from $\hat{Z}^{Y_{\tau_2}}$, which maximizes the coefficient $\text{Corr}(X, \hat{X}^{\hat{Z}^{Y_{\tau_2}}})$. Denoting the obtained mapping by $\hat{X}^{\hat{Z}^Y}$, which is acquired from a successive MCM procedure and characterizes the indirect information flow through Z , and then obtaining \hat{X}^Y , which characterizes all causal information from X to Y , by repeating the above procedure to time series pair X and the translated Y_{τ_1} , we introduce the correlation index: $q_D = \left| \text{Pcc}(X, \hat{X}^Y | \hat{X}^{\hat{Z}^Y}) \right|$ to measure the direct causation from X to Y conditioned on the indirect causation through Z , where $\text{Pcc}(\cdot, \cdot | \cdot)$ is the partial correlation coefficient describing the association degree between the first two variables with information about the third variable removed⁴⁴, in contrast to the MCM index $q_C = \left| \text{Corr}(X, \hat{X}^Y) \right|$. Note that we search for the strongest causation on different candidate time delays in every MCM procedure above. As a consequence, q_D can be regarded intuitively as the projection of q_C onto the information space orthogonal to the indirect information $\hat{X}^{\hat{Z}^Y}$ (Fig. 2b), and thus eliminates the indirect causal influence.

For three causally interacting variables X , Y , and Z , we generally have $q_C \geq q_D$. Setting an empirical threshold $1 > T \gg 0$, we have three cases for the order of the correlation index: $q_C \geq q_D \geq T$, $q_C \geq T \gg q_D$, and $T > q_C \geq q_D$, corresponding, respectively, to the three causal relations: a direct causal link from X to Y , a sole indirect causal link from X to Y , and the absence of any causal link from X to Y . The index q_D thus characterizes the degree to which direct causal links can be ascertained while eliminating the possibility of indirect links. For the example in Fig. 2a, the causal interaction of X and Y belongs to the second case above, which can be inferred from the correlation index in the same order as $q_C \geq T \gg q_D$. In real applications, it can happen that the causal signals in transition are not strong enough, making the values of $q_C \gtrsim T$ and q_D close to that of T . In such a case, the detection of direct causal links becomes more sensitive to the value of T . To overcome this difficulty, we introduce $\gamma = q_D/q_C$ to measure the proximity of the two index values. The closer the proximity to one, the higher the possibility of the existence of a direct causal link. Multiple tests^{45–47} have been conducted to ensure statistical reliability.

The framework of PCM can be generalized to networked systems with an arbitrary number of interacting variables: X , Y , Z^1 , ..., Z^s ($s \geq 2$) (e.g., Fig. 1d). With the full correlation between X and \hat{X}^Y , we calculate their partial correlation coefficient, denoted as $q_{D_1} = \left| \text{Pcc}(X, \hat{X}^Y | \{\hat{X}^{\hat{Z}^{iY}} | i = 1, \dots, s\}) \right|$, by removing the information of the cross mapping variables from the s variables Z^1 , ..., Z^s , where q_{D_1} is a first-order measure for distinguishing the direct from indirect causal link from X to Y . Motivation and formalization for extending this measure to higher orders is described in “Methods” section. We emphasize here that strongly coupled (synchronized) variables in nonlinear systems are not in the scope of the PCM framework, because in this circumstance the complete system collapses to the cause system sub-manifold, and the effect variable becomes an observation function on the cause system, where bidirectional

causation will always be computationally detected¹⁷. In addition, theoretically our PCM framework is based on the Takens–Mañé theorem, which is applicable only for autonomous systems. Data entirely recorded from nonautonomous systems are therefore not directly suitable for this framework⁴⁸, but our method can be applied to some nonautonomous systems. In particular, it can be numerically used to detect piecewise causations with data from switching systems where the switching points could be located and each duration between the consecutive switching points is sufficiently long. Also, our framework is suitable for some forced systems or/and systems with weak or moderate noise because some generalized embedding theorems could support the soundness of our framework^{49,50}. As for an important kind of nonautonomous system, viz., dynamical oscillators with time-evolving coupled functions or/and with various types of noise, the dynamical Bayesian inference with a delicate set of function bases can provide pretty practical solutions¹⁴. As for the future research topics, possible investigations include combining the above mutually complementary methods for causation detection in more general dynamical systems without knowing explicit model equations but with highly complex interaction structures.

Ascertaining direct causation in benchmark systems. To validate our PCM method, we use the following benchmark system of three interacting species: $x_t = x_{t-1}(\alpha_x - \alpha_{xy}x_{t-1} - \beta_{xy}y_{t-1}) + \epsilon_{x,t}$, $y_t = y_{t-1}(\alpha_y - \alpha_{yx}y_{t-1} - \beta_{yx}x_{t-1} - \beta_{yz}z_{t-1}) + \epsilon_{y,t}$, and $z_t = z_{t-1}(\alpha_z - \alpha_{zx}z_{t-1} - \beta_{zx}x_{t-1}) + \epsilon_{z,t}$ for $\alpha_x = 3.6$, $\alpha_y = 3.72$, and $\alpha_z = 3.68$, where $\epsilon_{i,t}$ ($i \in \{x, y, z\}$) are white noise of zero mean and standard deviation 0.005. Different choices of the coupling parameters β_{xy} , β_{yx} , β_{yz} , and β_{zx} can lead to distinct interacting modes (Fig. 3a). From the time series, we compute the MCM and PCM indices, q_C and q_D , respectively, for detecting the causal link from X to Y , with results listed in Fig. 3b, c. While there are cases where both methods are effective at detecting the direct causal links, for the causal chain and the causal loop structures with the threshold value $T = 0.5$, the PCM method succeeds in discriminating the indirect causal links, while clearly the MCM method, without eliminating the influence of the causation transitivity, fails. As further shown in Supplementary Note 2, the PCM performance is more robust than that of the MCM method with respect to variations in the value of T , making the PCM method applicable to real-world systems when there is none or little a priori knowledge of assigning a proper value of T . The results in Fig. 3b, c have also been verified by using the multi-testing corrections. Additionally, for all the other possible interaction structures of three species, including the representative network motifs: fan-in, fan-out, and cascading structures^{51,52}, our systematic studies manifest that the PCM method achieves accurate causation detections completely (see Supplementary Note 1). More importantly, we systematically conducted comparison studies with the Granger causality, the transfer entropy and all their conditional extensions to detect the causations for the above three species system and tested their robustness against different noise levels and time series lengths. As clearly shown in Supplementary Note 3, the PCM outperforms those existing methods which are, in principle, suitable only for the variables satisfying the separability condition. We also provided a comparison study between the PCM framework and the dynamical Bayesian inference in Supplementary Note 3. Both methods have their own particular advantages and could be used in a complementary manner. All these results systematically demonstrate the universal and peculiar usefulness of our method to the typical situation where the variables of dynamical systems are non-separable.

Additionally, we validate the effectiveness of the PCM method in a network model containing eight interacting species. As

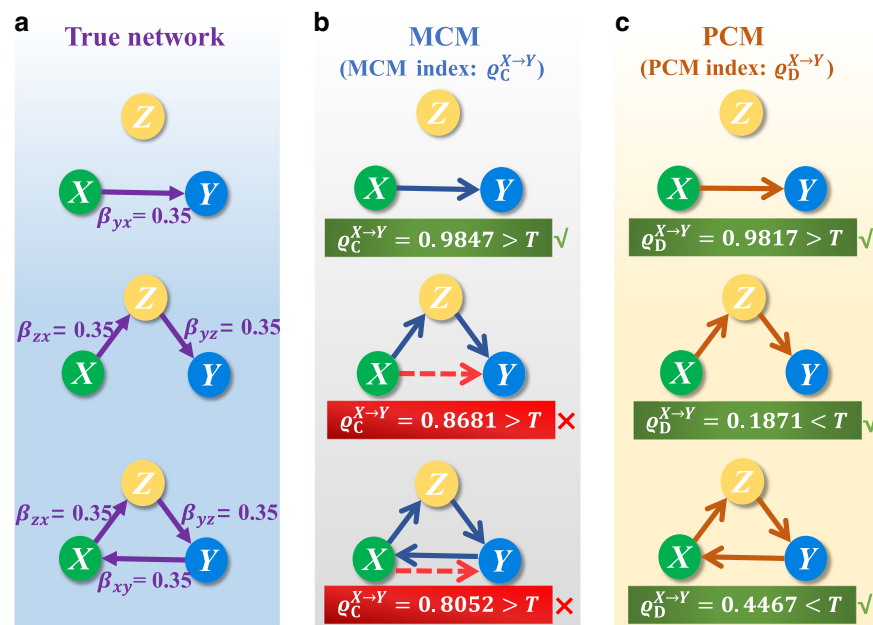


Fig. 3 Detection of causal links from X to Y in the benchmark systems. **a** Three distinct interaction modes of the system. **b** Causal links from X to Y detected by the MCM method, which contain false direct causation for the second and the third interaction modes. **c** Direct causal links detected by the PCM method, which successfully excludes the false direct causations in **b**. Randomly selected are the 100 trials with a 1000-length from 5000-length time series, where the sampling rate is 1 Hz so that the length matches exactly the time unit of the system. The average is calculated over the results of these randomly selected trials. The phase-space reconstruction parameters are $E = 4$ and $\tau = 1$. Here superscripts of q_C and q_D denote the specified causal direction.

shown in Supplementary Fig. 10, the direct causal network can be reconstructed faithfully while the indirect links are all eliminated successfully with setting an appropriate group of T . In contrast, with the same values of T , the MCM method produces a dense network containing direct, indirect, and even erroneous causal links. We also find that the ratio $\gamma = q_D/q_C$ can be used to improve the detection accuracy even for relatively small values of the threshold T (Supplementary Note 4). Moreover, selecting a practically effective threshold value is much more realizable and robust in our PCM method (see Supplementary Fig. 11 and see Supplementary Note 5 for detailed information on statistical tests and methods for threshold selection). The robustness tests of PCM against the time series lengths and the noise scales also show good effectiveness even with small data size and relatively strong noise in this model (Supplementary Note 3). These additional results demonstrate the power of our PCM method in detecting direct links and accurately reconstructing the underlying causal networks from multivariate time series.

Detecting direct causation in real-world networks. We test gene regulatory networks with gene expression data available from DREAM4 in silico Network Challenge^{53–55}. There are five networks with different, synthetically produced structures. Each network has 100 genes. We use the software GeneNetWeaver⁵⁶ to randomly select 20 interacting genes, where each gene has 10 realizations of 21 gene expression time series data. Figure 4a presents one gene regulatory network (see Supplementary Fig. 12 for the others). For each gene, we combine all realizations as one time series for phase-space reconstruction. We compare the direct causal links detected by PCM with the a priori known edges of the five networks and calculate the respective ROC (receiver operating characteristic) curves (Fig. 4b). We find the average of the five areas under the ROC curves approaches the value of ~ 0.75 , indicating high detection accuracies of direct links in gene

regulatory networks even with small data sets, a task for which PCM outperforms the MCM method (see Supplementary Note 6).

We next consider the food chain network of three plankton species: *Pico cyanobacteria*, *Rotifers* and *Cycloids*, with the prey–predator relations indicated in Fig. 4c. The oscillatory population data are selected from an 8-year mesocosm experiment of a plankton community isolated from the Baltic Sea^{57–59}. Our PCM method yields six indices for all the possible causal links, and we preserve the links with index values $\gtrsim 10^{-1}$ and discard other links (see Supplementary Note 5 for issues on threshold selection). This leads to two direct causal links, which agree with the ground truth of the original network (Fig. 4d). Remarkably, our PCM method successfully excludes the indirect link from *Pico cyanobacteria* to *Cycloids*. For this network, there is also a weak direct link from *Rotifers* to *Pico cyanobacteria*, and our method is indeed able to detect it (verified with multi-testing corrections). This reveals that the actual prey–predator hierarchy does not necessarily match the direct causal links among the species. For example, while predators hunt preys, a predator through hunting can significantly influence the prey populations when they are not tremendously abundant. In such a case, the predator can be regarded as the causal source, giving rise to the third relatively weak but direct causal link.

Our third real-world example is from the recorded data of air pollution and hospital admission of cardiovascular diseases in Hong Kong from 1994 to 1997 (see Supplementary Note 6)^{60–62}. As shown in Fig. 4e, f, our PCM method uncovers that only the pollutants, that is, nitrogen dioxide and respirable suspended, are detected as the major causes of cardiovascular diseases. Neither sulfur dioxide nor ozone has been identified as the cause for the diseases, which is consistent with previous results^{20,63}. Our method reveals a unidirectional causal relation from ozone to sulfur dioxide, but the detected causal relations among the recognized pollutants are bidirectional. It is likely that these detected causal relations are either direct or indirect, because data

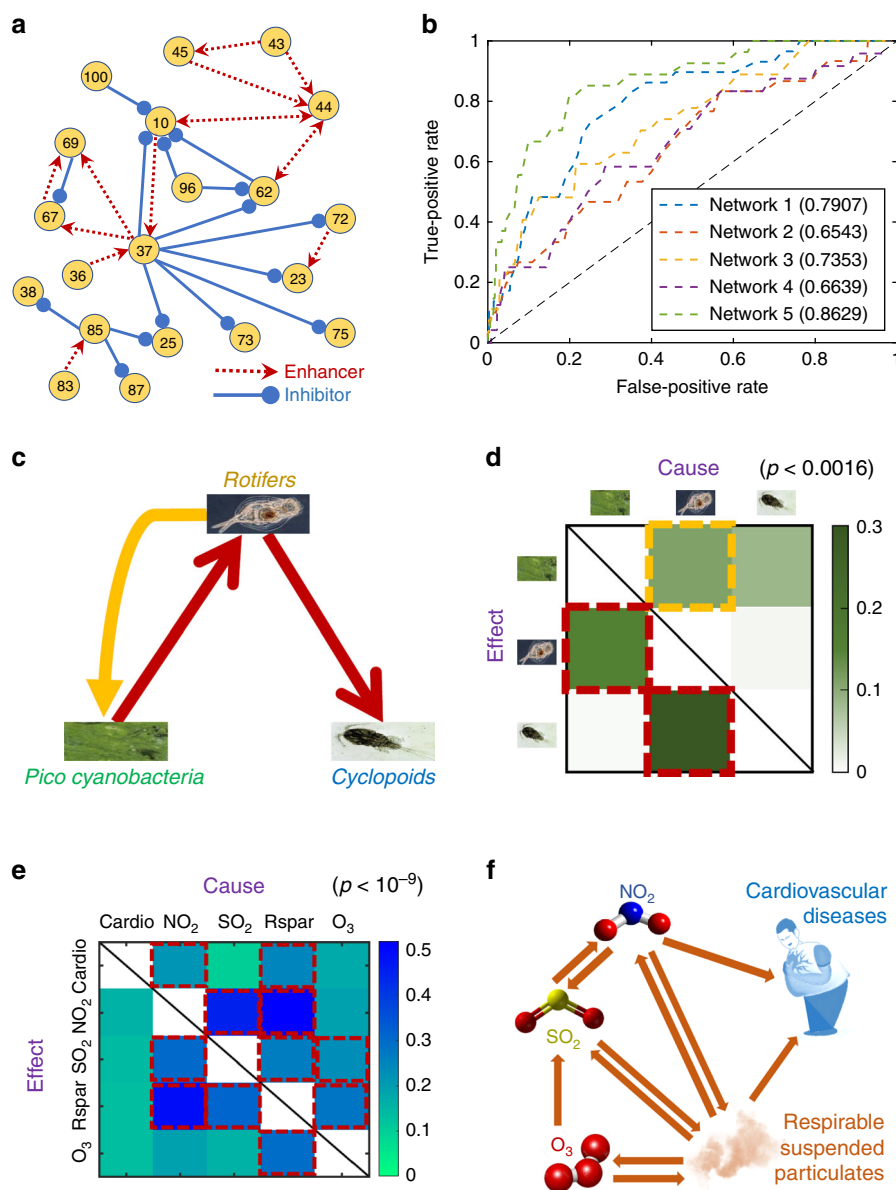


Fig. 4 Detecting direct causal links in three real-world networks. **a** One of the five gene regulatory networks with 20 interacting genes from GeneNetWeaver. Each red (blue) arrow represents an activating (inhibitory) effect. **b** ROC curves characterizing the PCM detection performance. The corresponding AUROCs are also indicated. The reconstruction parameters are $E = 2$ and $\tau = 1$. **c** A food chain network of three plankton species, where the direction of each red arrow represents a prey to predator interaction. **d** The PCM indices (the color region framed by red boxes) signifying successful detection of the direct causal links (for $E = 4$ and $\tau = 1$). A relatively weak but direct causal link (the yellow arrow in **c**) from *Rotifers* to *Pico cyanobacteria* is identified through the index framed by the yellow box. **e** Results on all successfully detected interactions between air pollutants and cardiovascular diseases (red box) for $E = 7$ and $\tau = 1$. **f** The reconstructed causal network from the results in **e**. All detection results are verified using multiple testing corrections.

of other factors, such as temperature, humidity, and wind speed, are not completely available, which can be the common causes to some pollutants (e.g., the fan-out interaction mode shown in Supplementary Fig. 2).

We also apply the PCM method to real-world examples, including gene expression data related to the circadian rhythms and electroencephalography data of the human brain in Supplementary Note 7. All the results demonstrate the broad applicability of our method to different scales of data sets, and indeed reveal new viewpoints to the dynamical underpinnings of real-world systems.

Discussion

To summarize the work, by exploiting both dynamical and statistical features from the observed data, there are two major

advantages of our method: detecting direct causality based on PCM and handling non-separability problem based on Takens–Mañé’s embedding theorem. Actually, variables for a nonlinear dynamical system are generally considered non-separable due to their intertwined nonlinear nature. Specifically, in contrast to the existing methods on detecting causation, which either misidentify indirect causal links as direct ones or fail due to a violation of the condition of separability, we develop a method theoretically and computationally to solve this outstanding problem, coping with the situation for which the existing frameworks cannot work effectively. The central idea lies in examining the consensus between one time series and its cross map prediction from the other with conditioning on the part that is transferred from the third variable. Our method is capable of not only distinguishing direct from indirect causal

influences but also removing the latter. A virtue of our method is that it is generally applicable to nonlinear dynamical networks without requiring the condition of separability, which complements the missing part of causality analysis (see Supplementary Table 3). In fact, the concept of causality in dynamical systems is different from the widely accepted traditional statistical viewpoint that X causes Y if and only if an intervention in X has an effect on Y . Due to the non-separability, causality in dynamical systems should have different formalization, which in simplest way can be intuitively interpreted as a coupling term from X to Y in the system's equations. Further theoretical interpretations regarding this new framework will be included in our future work. Finally, our PCM method is validated by applying to a number of real-world systems, yielding new insights into the dynamics of these systems. Unambiguous identification of direct causal links with indirect causal influence eliminated is a key to understanding and accurately modeling the underlying system, and our framework therefore provides a vehicle to achieve this goal.

Methods

The concept of non-separability. We illustrate the concept, non-separability, by using a general continuous-time dynamical system:

$$\dot{\mathbf{x}} = F(\mathbf{x}), \tag{1}$$

where the state variable $\mathbf{x}(t) = [x_1(t), x_2(t), \dots, x_n(t)]^\top$ evolves inside a compact manifold \mathcal{M}_x , forming an attractor \mathcal{A} with a dimension d_A . Here, d_A can be computed as the box-counting dimension of \mathcal{A} . The dynamics with an initial value $\mathbf{x}_0 \in \mathcal{M}_x$ are denoted by $\mathbf{x}(t) = \varphi_t(\mathbf{x}_0)$, where $\varphi_t(\cdot)$ is regarded as a flow along the manifold \mathcal{M}_x . According to Takens–Mañé’s embedding theory and its fractal generalizations, one can, with probability one, reconstruct the system with a positive delay τ and a smooth observation function $h : \mathcal{M}_x \rightarrow \mathbb{R}$ in the sense that the delay-coordinate map $\Gamma_{h, \varphi_\tau}(\mathbf{x}) = [h(\mathbf{x}), h(\varphi_{-\tau}(\mathbf{x})), h(\varphi_{-2\tau}(\mathbf{x})), \dots, h(\varphi_{-(L-1)\tau}(\mathbf{x}))]^\top$ is generically an embedding map as long as $L > 2d_A$. Particularly for direct illustration, we take the observation function $h(\mathbf{x})$ as a simple coordinate function: $h(\mathbf{x}) = x_i$, where x_i is the i th component of \mathbf{x} . Thus, we have $\mathbf{y}(t) = [x_i(t), x_i(t - \tau), \dots, x_i(t - (L - 1)\tau)]^\top$ and also have the manifold \mathcal{M}_x mapped to the shadow manifold \mathcal{M}_y by the embedding map Γ . Since the embedding map is one to one, the dynamics ψ_τ on the shadow manifold \mathcal{M}_y are topologically conjugated with the dynamics φ_τ on \mathcal{M}_x , that is,

$$\mathbf{y}(t + \tau) = \psi_\tau(\mathbf{y}(t)) = \Gamma \circ \varphi_\tau \circ \Gamma^{-1}(\mathbf{y}(t)). \tag{2}$$

On the one hand, system (1) implies a fact that the future dynamics of one specific component, say x_j with $j =$ (or \neq) i , is governed by

$$[\varphi_\tau]_j : \mathbf{x}(t) = [x_1(t), x_2(t), \dots, x_n(t)]^\top \rightarrow x_j(t + \tau) \tag{3}$$

and thus depends on the history of all the components x_1, x_2, \dots, x_n . On the other hand, the relation in (2) implies the other fact that as long as the embedding map Γ exists, the future dynamics of x_j is also governed by

$$[\Gamma^{-1} \circ \psi_\tau]_j : \mathbf{y}(t) = [x_i(t), x_i(t - \tau), \dots, x_i(t - (L - 1)\tau)]^\top \rightarrow x_j(t + \tau) \tag{4}$$

and thus only depends on the history of one variable x_i and on the embedding map Γ as well.

Generically, it is possible to make a prediction of $x_j(t + \tau)$ based only on the observation of one variable, and this prediction could be as perfect as the prediction using the information of all the variables $x_1(t), x_2(t), \dots, x_n(t)$ of the system (this obviously disables the idea of Granger causality and its extensions). Thus, Takens–Mañé’s embedding theory reveals that, in such a deterministic nonlinear dynamical system, the information of the whole dynamical system could be generically injected into only one single variable and thus could be reconstructed by the observation data of that variable. This therefore invites a concept of non-separability, that is, one, prevalently, cannot remove the information of some variable from the other variables when any prediction is made for the dynamical systems. This also reveals that the methods based on prediction frameworks, such as the Granger causality, the transfer entropy, and all their extensions, mathematically are not suitable for dealing with the time series data produced by nonlinear dynamical systems where non-separability always exists among the internal variables. A toy example showing how GC fails in non-separable systems could be referred to the Supplementary Materials of ref. 17.

Transitivity arousing indirect causation. To investigate how the transitivity arouses indirect causation, we consider a heuristic logistic model of three species

connected in the following manner:

$$\begin{aligned} x_t &= x_{t-1}(\alpha_x - \alpha_x x_{t-1}), \\ z_t &= z_{t-1}(\alpha_z - \alpha_z z_{t-1} - \beta_{zx} x_{t-1}), \\ y_t &= y_{t-1}(\alpha_y - \alpha_y y_{t-1} - \beta_{yz} z_{t-1}), \end{aligned} \tag{5}$$

where the three species $X = \{x_t\}$, $Z = \{z_t\}$ and $Y = \{y_t\}$ are interacting in a causal chain, denoted by $X \rightarrow Z \rightarrow Y$, and the coupling strengths β_{zx} and β_{yz} are nonzero.

Now, we shift the second equation in (5) with one time step and then substitute it into the last equation in (5), which yields:

$$y_t = y_{t-1} [\alpha_y - \alpha_y y_{t-1} - \beta_{yz} z_{t-2} (\alpha_z - \alpha_z z_{t-2} - \beta_{zx} x_{t-2})]. \tag{6}$$

Also the last equation in (5) can be transformed as:

$$z_{t-1} = \frac{1}{\beta_{yz}} (\alpha_y - \alpha_y y_{t-1} - y_t / y_{t-1}), \tag{7}$$

so that

$$z_{t-2} = \frac{1}{\beta_{yz}} (\alpha_y - \alpha_y y_{t-2} - y_{t-1} / y_{t-2}). \tag{8}$$

Then, a substitution of Eq. (8) into Eq. (6) gives:

$$\begin{aligned} y_t &= y_{t-1} \left\{ \alpha_y - \alpha_y y_{t-1} - \beta_{yz} \frac{1}{\beta_{yz}} (\alpha_y - \alpha_y y_{t-2} - y_{t-1} / y_{t-2}) \right. \\ &\quad \left. \times \left[\alpha_z - \alpha_z \frac{1}{\beta_{yz}} (\alpha_y - \alpha_y y_{t-2} - y_{t-1} / y_{t-2}) - \beta_{zx} x_{t-2} \right] \right\}. \end{aligned} \tag{9}$$

Consequently, this equation, coupling with the first equation in (5), forms a causation relation unidirectionally from X to Y . However, this causation is indirect, induced by the transitivity, and then the influence has the effect of time delay for discrete-time dynamical systems.

The PCM method of first order and higher order. We now formulate the PCM framework formally (see Supplementary Fig. 1 for a schematic graph of the PCM procedure). The first step is to translate the time series $Y = \{y_t\}$ with time steps $\tau_i (i = 1, 2, \dots, m)$, generating m translated variables denoted as $Y_{\tau_i} = \{y_{t+\tau_i}\}$. For time series pair Y_{τ_i} and Z , we apply the conventional MCM method (see the practical steps below) to obtain the mapping $\hat{Z}^{Y_{\tau_i}}$ from Y_{τ_i} and calculate the correlation coefficient $\text{Corr}(Z, \hat{Z}^{Y_{\tau_i}})$. For simplicity, we denote \hat{Z}^Y as the mapping $\hat{Z}^{Y_{\tau_i}}$ with

$$i_1 = \text{argmax}_{1 \leq i \leq m} \text{Corr}(Z, \hat{Z}^{Y_{\tau_i}}). \tag{10}$$

The next step is to repeat the procedure to the time series pair of translated $\hat{Z}^{Y_{\tau_i}}$ and X so as to obtain the mapping $\hat{X}^{\hat{Z}^{Y_{\tau_i}}}$ from $\hat{Z}^{Y_{\tau_i}}$, and set $\hat{X}^{\hat{Z}^Y}$ as $\hat{X}^{\hat{Z}^{Y_{\tau_{i_2}}}}$ with

$$i_2 = \text{argmax}_{1 \leq i \leq m} \text{Corr}(X, \hat{X}^{\hat{Z}^{Y_{\tau_i}}}). \tag{11}$$

Now the obtained $\hat{X}^{\hat{Z}^Y}$ represents the indirect information flow. By directly applying MCM to the translated Y_{τ_i} and X , we could have \hat{X}^Y denoting all the information transferred from X to Y , which is simplified for $\hat{X}^{Y_{\tau_{i_3}}}$ with

$$i_3 = \text{argmax}_{1 \leq i \leq m} \text{Corr}(X, \hat{X}^{Y_{\tau_i}}). \tag{12}$$

We now introduce the correlation index:

$$Q_D = \left| \text{Pcc}(X, \hat{X}^Y | \hat{X}^{\hat{Z}^Y}) \right|, \tag{13}$$

where $\text{Pcc}(\cdot, \cdot | \cdot)$ is the partial correlation coefficient describing the association degree between the first two variables with information about the third variable removed. We review the definition of partial correlation coefficient here. For time series X, Y , and Z^1, \dots, Z^l , the partial correlation coefficient between X and Y conditioned on Z^1 is

$$\text{Pcc}(X, Y | Z^1) = \frac{\text{Corr}(X, Y) - \text{Corr}(X, Z^1)\text{Corr}(Y, Z^1)}{\sqrt{(1 - \text{Corr}(X, Z^1)^2)(1 - \text{Corr}(Y, Z^1)^2)}}. \tag{14}$$

The partial correlation coefficient between X and Y conditioned on both Z^1 and Z^2 is

$$\text{Pcc}(X, Y | Z^1, Z^2) = \frac{\text{Pcc}(X, Y | Z^1) - \text{Pcc}(X, Z^2 | Z^1)\text{Pcc}(Y, Z^2 | Z^1)}{\sqrt{(1 - \text{Pcc}(X, Z^2 | Z^1)^2)(1 - \text{Pcc}(Y, Z^2 | Z^1)^2)}}, \tag{15}$$

and the partial correlation coefficient between X and Y conditioned on more variables can be defined recursively. For the computation and more information on the partial correlation coefficient, see refs. 44,64.

To provide detailed instruction to our method, we summarize the practical steps here:

Procedure A: MCM for detecting causation from $U = \{u_t\}_{t=1}^L$ to $V = \{v_t\}_{t=1}^L$:

1. Reconstruct the phase space by using delay-coordinate embedding for time series U and V , the reconstruction parameters (embedding dimensions E_u, E_v , and time lags τ_u, τ_v) can be selected by FNN algorithm and by the method of DMI, respectively (see Supplementary Note 5);
2. For each time index t , find the set of neighboring points $\mathcal{N}(\mathbf{v}_t)$ of \mathbf{v}_t ($E_v + 1$ nearest neighbors are used since it is the minimum number of points needed for a bounded simplex in an E_v -dimensional space⁴³);
3. Find the corresponding points in M_U that have the same time indexes as the points in $\mathcal{N}(\mathbf{v}_t)$ and calculate their weighted average (the weights are determined by the distances between the point in $\mathcal{N}(\mathbf{v}_t)$ and \mathbf{v}_t , which defines the operation $\mathbb{E}[\cdot]$) to obtain the estimated $\hat{\mathbf{u}}_t^Y$;
4. Use an appropriate index (such as $q_C = |\text{Corr}(\mathbf{u}_t, \hat{\mathbf{u}}_t^Y)|$) to characterize the consensus of the estimated time series \hat{U}^{V_0} (subscript 0 is denoted for no translation of V here to keep consistency with the following notations) and the original time series U , which measures the causation from U to V .

Procedure B: PCM for detecting direct causation from X to Y conditioning on Z :

1. Translate time series Y with different candidate time delays $\tau_i (i = 1, 2, \dots, m)$ to generate $Y_{\tau_i} = \{y_{t+\tau_i}\}$;
2. For each pair Z to Y_{τ_i} , perform Procedure A to obtain $\text{Corr}(Z, \hat{Z}^{Y_{\tau_i}})$, and denote \hat{Z}^Y as $\hat{Z}^{Y_{\tau_i}}$, where the time delay τ_i maximizes $\text{Corr}(Z, \hat{Z}^{Y_{\tau_i}})$ as in (10);
3. Translate time series \hat{Z}^Y with different candidate time delays $\tau_i (i = 1, 2, \dots, m)$ to generate $\hat{Z}_{\tau_i}^Y$;
4. For each pair X to $\hat{Z}_{\tau_i}^Y$, perform Procedure A to obtain $\text{Corr}(X, \hat{X}^{\hat{Z}_{\tau_i}^Y})$, and denote $\hat{X}^{\hat{Z}^Y}$ as $\hat{X}^{\hat{Z}_{\tau_i}^Y}$, where the time delay τ_i maximizes $\text{Corr}(X, \hat{X}^{\hat{Z}_{\tau_i}^Y})$ as in (11);
5. For each pair X to Y_{τ_i} , perform Procedure A to obtain $\text{Corr}(X, \hat{X}^{Y_{\tau_i}})$, and denote \hat{X}^Y as $\hat{X}^{Y_{\tau_i}}$, where the time delay τ_i maximizes $\text{Corr}(X, \hat{X}^{Y_{\tau_i}})$ as in (12);
6. Use $q_D = \left| \text{Pcc}(X, \hat{X}^Y | \hat{X}^{\hat{Z}^Y}) \right|$ to measure the direct causation from X to Y conditioning on Z .

Note that we search for the strongest causation on different candidate time delays in every MCM procedure above. For consistency, in the whole research, all the MCM results are also based on this strategy. Moreover, it is possible to characterize the causal relations among variables on a distribution of time delays (i.e., a causal spectrum). This full causal description will be included in our future work.

As described above, the first-order PCM method can be established as following definition for networked systems of more than three interacting variables: $X, Y, Z^1, \dots, Z^s (s \geq 2)$ (e.g., Fig. 1d), based on which high-order method can be derived,

$$q_{D_1} = \left| \text{Pcc} \left(X, \hat{X}^Y \left| \left\{ \hat{X}^{Z^i} \mid i = 1, \dots, s \right\} \right. \right) \right|. \tag{16}$$

In a complex dynamical networks, the indirect causation could also be transferred through more than one variables (e.g., through two variables $X \rightarrow Z^1 \rightarrow Z^2 \rightarrow Y$). The high-order PCM method is derived to specifically characterize this situation. In particular, we calculate the correlation coefficient between X and \hat{X}^Y , and the partial correlation coefficient between them through removal of the information about the cross mapping variables via two variables out of the s variables Z^1, \dots, Z^s . The partial correlation coefficient

$$q_{D_2} = \left| \text{Pcc} \left(X, \hat{X}^Y \left| \left\{ \hat{X}^{Z^i} \mid i \neq j, i, j \in \{1, \dots, s\} \right\} \right. \right) \right| \tag{17}$$

represents effectively a second-order method for differentiating the direct and indirect causal links from X to Y that is transferred through two mediate variables. Analogously, the n th order measure, denoted by q_{D_n} , can be defined through any combinations of n mediate variables from Z^1, \dots, Z^s as

$$q_{D_n} = \left| \text{Pcc} \left(X, \hat{X}^Y \left| \left\{ \hat{X}^{Z^i} \mid (i_1, \dots, i_n) \text{ is an } n\text{-combination from } \{1, \dots, s\} \right\} \right. \right) \right|. \tag{18}$$

Together with $q_C, q_{D_n} (n = 1, \dots, s)$ and the PCM measure

$$\gamma = (\prod_{n=1}^s q_{D_n}) / q_C^s, \tag{19}$$

reflecting the proximity of all these coefficients, we obtain higher-order PCM methods for detecting direct causal links in large networks. However, for a relatively large order n , the possible number of combinations of n mediate variables is quite large. We will study the computations and applications of the high-order methods in future work, and in this research, we only consider the first-order problem.

In practice, the partial correlation procedure will encounter calculation problems if the network scale is relatively large and thus a large conditioning set should be taken into account. In this case, we could adopt the technique of selecting several nodes Z^i that maximize $q_C^{X \rightarrow Z^i} + q_C^{Z^i \rightarrow Y}$ (or $\min\{q_C^{X \rightarrow Z^i}, q_C^{Z^i \rightarrow Y}\}$), which means a high probability of the existence of an indirect link through Z^i , and

make conditioning on these nodes. Moreover, if we have a priori knowledge that the network is sparse, that is, indirect connections are seldom, we could also make conditioning on Z^1, \dots, Z^s one by one, and take the minimum value of $q_D^{X \rightarrow Y | Z^i}$ as the final result.

Moreover, the PCM idea can be further developed or varied by substituting the partial correlation to other possible measures characterizing the conditional dependence. For example, the coefficient of determination (denoted r^2) is a possible choice to serve as an index directly estimated from the cross map neighbors in parceling out effect sizes for each contributing factor. Another heuristic thinking is that for indirect causal influence $X \rightarrow Z \rightarrow Y$, cutting off either the link $X \rightarrow Z$ or $Z \rightarrow Y$ is enough to eliminate the whole indirect information flow, which also provides variation of the PCM framework. These further variations will be included in our future work.

Data availability

The data sets generated during and/or analyzed during the current study are all available from the corresponding author on reasonable request. The links/references for the public data sets used and analyzed during the current study are all provided in Supplementary Information.

Code availability

The codes as well as their directions for the PCM framework that we developed in this article are publicly available at <https://github.com/Partial-Cross-Mapping>.

Received: 3 December 2019; Accepted: 22 April 2020;

Published online: 26 May 2020

References

1. Granger, C. W. Investigating causal relations by econometric models and cross-spectral methods. *Econometrica* **37**, 424–438 (1969).
2. Geweke, J. F. Measurement of linear dependence and feedback between multiple time series. *J. Am. Stat. Assoc.* **77**, 304–313 (1982).
3. Geweke, J. F. Measures of conditional linear dependence and feedback between time series. *J. Am. Stat. Assoc.* **79**, 907–915 (1984).
4. Ding, M., Chen, Y. & Bressler, S. L. In *Handbook of Time Series Analysis* 437–460 (Wiley, Hoboken, 2006).
5. Guo, S., Ladrone, C. & Feng, J. In *Frontiers in Computational and Systems Biology* 83–111 (Springer, New York, 2010).
6. Schreiber, T. Measuring information transfer. *Phys. Rev. Lett.* **85**, 461 (2000).
7. Vicente, R., Wibral, M., Lindner, M. & Pipa, G. Transfer entropy—a model-free measure of effective connectivity for the neurosciences. *J. Comput. Neurosci.* **30**, 45–67 (2011).
8. Cover, T. M. & Thomas, J. A. *Elements of Information Theory* (Wiley, Hoboken, 2012).
9. Sun, J., Cafaro, C. & Bollt, E. M. Identifying the coupling structure in complex systems through the optimal causation entropy principle. *Entropy* **16**, 3416–3433 (2014).
10. Cafaro, C., Lord, W. M., Sun, J. & Bollt, E. M. Causation entropy from symbolic representations of dynamical systems. *Chaos* **25**, 043106 (2015).
11. Sun, J., Taylor, D. & Bollt, E. M. Causal network inference by optimal causation entropy. *SIAM J. Appl. Dyn. Syst.* **14**, 73–106 (2015).
12. Duggento, A., Stankovski, T., McClintock, P. V. & Stefanovska, A. Dynamical bayesian inference of time-evolving interactions: from a pair of coupled oscillators to networks of oscillators. *Phys. Rev. E* **86**, 061126 (2012).
13. Stankovski, T., Duggento, A., McClintock, P. V. & Stefanovska, A. A tutorial on time-evolving dynamical bayesian inference. *Eur. Phys. J. Spec. Top.* **223**, 2685–2703 (2014).
14. Stankovski, T., Ticcinielli, V., McClintock, P. V. & Stefanovska, A. Coupling functions in networks of oscillators. *N. J. Phys.* **17**, 035002 (2015).
15. Stankovski, T., Pereira, T., McClintock, P. V. & Stefanovska, A. Coupling functions: universal insights into dynamical interaction mechanisms. *Rev. Mod. Phys.* **89**, 045001 (2017).
16. Schiff, S. J., So, P., Chang, T., Burke, R. E. & Sauer, T. Detecting dynamical interdependence and generalized synchrony through mutual prediction in a neural ensemble. *Phys. Rev. E* **54**, 6708 (1996).
17. Sugihara, G. et al. Detecting causality in complex ecosystems. *Science* **338**, 496–500 (2012).
18. Ma, H., Aihara, K. & Chen, L. Detecting causality from nonlinear dynamics with short-term time series. *Sci. Rep.* **4**, 7464 (2014).
19. Jiang, J.-J., Huang, Z.-G., Huang, L., Liu, H. & Lai, Y.-C. Directed dynamical influence is more detectable with noise. *Sci. Rep.* **6**, 24088 (2016).
20. Ma, H. et al. Detection of time delays and directional interactions based on time series from complex dynamical systems. *Phys. Rev. E* **96**, 012221 (2017).

21. Harnack, D., Laminski, E., Schünemann, M. & Pawelzik, K. R. Topological causality in dynamical systems. *Phys. Rev. Lett.* **119**, 098301 (2017).
22. Joskow, P. L. & Rose, N. L. In *Handbook of Industrial Organization*, Vol. 2, 1449–1506 (Elsevier, Amsterdam, 1989).
23. Kamiński, M., Ding, M., Truccolo, W. A. & Bressler, S. L. Evaluating causal relations in neural systems: Granger causality, directed transfer function and statistical assessment of significance. *Biol. Cybern.* **85**, 145–157 (2001).
24. Banos, R. et al. Optimization methods applied to renewable and sustainable energy: a review. *Renew. Sust. Energ. Rev.* **15**, 1753–1766 (2011).
25. Brockmann, D. & Helbing, D. The hidden geometry of complex, network-driven contagion phenomena. *Science* **342**, 1337–1342 (2013).
26. Deyle, E. R. et al. Predicting climate effects on pacific sardine. *Proc. Natl Acad. Sci. USA* **110**, 6430–6435 (2013).
27. Van Nes, E. H. et al. Causal feedbacks in climate change. *Nat. Clim. Change* **5**, 445 (2015).
28. Tsonis, A. A. et al. Dynamical evidence for causality between galactic cosmic rays and interannual variation in global temperature. *Proc. Natl Acad. Sci. USA* **112**, 3253–3256 (2015).
29. Hirata, Y. et al. Detecting causality by combined use of multiple methods: climate and brain examples. *PLoS ONE* **11**, e0158572 (2016).
30. Ma, H., Leng, S., Aihara, K., Lin, W. & Chen, L. Randomly distributed embedding making short-term high-dimensional data predictable. *Proc. Natl Acad. Sci. USA* **115**, E9994–E10002 (2018).
31. Leng, S., Xu, Z. & Ma, H. Reconstructing directional causal networks with random forest. *Chaos* **29**, 093130 (2019).
32. Guo, S., Seth, A. K., Kendrick, K. M., Zhou, C. & Feng, J. Partial granger causality-eliminating exogenous inputs and latent variables. *J. Neurosci. Methods* **172**, 79–93 (2008).
33. Frenzel, S. & Pompe, B. Partial mutual information for coupling analysis of multivariate time series. *Phys. Rev. Lett.* **99**, 204101 (2007).
34. Zhao, J., Zhou, Y., Zhang, X. & Chen, L. Part mutual information for quantifying direct associations in networks. *Proc. Natl Acad. Sci. USA* **113**, 5130–5135 (2016).
35. Runge, J., Heitzig, J., Petoukhov, V. & Kurths, J. Escaping the curse of dimensionality in estimating multivariate transfer entropy. *Phys. Rev. Lett.* **108**, 258701 (2012).
36. Schelter, B. et al. Direct or indirect? graphical models for neural oscillators. *J. Physiol.* **99**, 37–46 (2006).
37. Nawrath, J. et al. Distinguishing direct from indirect interactions in oscillatory networks with multiple time scales. *Phys. Rev. Lett.* **104**, 038701 (2010).
38. Runge, J. Causal network reconstruction from time series: from theoretical assumptions to practical estimation. *Chaos* **28**, 075310 (2018).
39. Runge, J., Petoukhov, V. & Kurths, J. Quantifying the strength and delay of climatic interactions: the ambiguities of cross correlation and a novel measure based on graphical models. *J. Clim.* **27**, 720–739 (2014).
40. Takens, F. In *Dynamical Systems and Turbulence, Warwick 1980*, 366–381 (Springer, New York, 1981).
41. Mañé, R. In *Dynamical Systems and Turbulence, Warwick 1980*, 230–242 (Springer, New York, 1981).
42. Kantz, H. & Schreiber, T. *Nonlinear Time Series Analysis*, Vol. 7 (Cambridge Univ. Press, Cambridge, 2004).
43. Sugihara, G. & May, R. M. Nonlinear forecasting as a way of distinguishing chaos from measurement error in time series. *Nature* **344**, 734 (1990).
44. Bailey, N. T. *Statistical Methods in Biology* (Cambridge Univ. Press, Cambridge, 1995).
45. Noble, W. S. How does multiple testing correction work? *Nat. Biotechnol.* **27**, 1135 (2009).
46. Shaffer, J. P. Multiple hypothesis testing. *Annu. Rev. Psychol.* **46**, 561–584 (1995).
47. Lancaster, G., Iatsenko, D., Pidde, A., Ticcinelli, V. & Stefanovska, A. Surrogate data for hypothesis testing of physical systems. *Phys. Rep.* **748**, 1–60 (2018).
48. Clemson, P. T. & Stefanovska, A. Discerning non-autonomous dynamics. *Phys. Rep.* **542**, 297–368 (2014).
49. Stark, J. Delay embeddings for forced systems. i. deterministic forcing. *J. Nonlinear Sci.* **9**, 255–332 (1999).
50. Stark, J., Broomhead, D. S., Davies, M. & Huke, J. Delay embeddings for forced systems. II. Stochastic forcing. *J. Nonlinear Sci.* **13**, 519–577 (2003).
51. Milo, R. et al. Network motifs: simple building blocks of complex networks. *Science* **298**, 824–827 (2002).
52. Alon, U. Network motifs: theory and experimental approaches. *Nat. Rev. Genet.* **8**, 450 (2007).
53. Marbach, D. et al. Revealing strengths and weaknesses of methods for gene network inference. *Proc. Natl Acad. Sci. USA* **107**, 6286–6291 (2010).
54. Marbach, D., Schaffter, T., Mattiussi, C. & Floreano, D. Generating realistic in silico gene networks for performance assessment of reverse engineering methods. *J. Comput. Biol.* **16**, 229–239 (2009).
55. Prill, R. J. et al. Towards a rigorous assessment of systems biology models: the dream3 challenges. *PLoS ONE* **5**, e9202 (2010).
56. Schaffter, T., Marbach, D. & Floreano, D. Genenetweaver: in silico benchmark generation and performance profiling of network inference methods. *Bioinformatics* **27**, 2263–2270 (2011).
57. Benincà, E., Jöhnk, K. D., Heerkloss, R. & Huisman, J. Coupled predator–prey oscillations in a chaotic food web. *Ecol. Lett.* **12**, 1367–1378 (2009).
58. Benincà, E. et al. Chaos in a long-term experiment with a plankton community. *Nature* **451**, 822 (2008).
59. Neutel, A.-M., Heesterbeek, J. A. & de Ruiter, P. C. Stability in real food webs: weak links in long loops. *Science* **296**, 1120–1123 (2002).
60. Lee, B.-J., Kim, B. & Lee, K. Air pollution exposure and cardiovascular disease. *Toxicol. Res. (Seoul, Repub. Korea)* **30**, 71 (2014).
61. Wong, T. W. et al. Air pollution and hospital admissions for respiratory and cardiovascular diseases in hong kong. *Occup. Environ. Med.* **56**, 679–683 (1999).
62. Fan, J. & Zhang, W. Statistical estimation in varying coefficient models. *Ann. Stat.* **27**, 1491–1518 (1999).
63. Milojevic, A. et al. Short-term effects of air pollution on a range of cardiovascular events in England and Wales: case-crossover analysis of the minap database, hospital admissions and mortality. *Heart* **100**, 1093–1098 (2014).
64. Baba, K., Shibata, R. & Sibuya, M. Partial correlation and conditional correlation as measures of conditional independence. *Aust. N. Z. J. Stat.* **46**, 657–664 (2004).

Acknowledgements

W.L. is supported by the National Key R&D Program of China (No. 2018YFC0116600), by the National Natural Science Foundation of China (Nos 11925103 and 61773125), and by the STCSM (Nos 18DZ1201000, 19511132000, and 2018SHZDZX01). L.N.C. is supported by the National Key R&D Program of China (No. 2017YFA0505500), by the Strategic Priority Project of CAS (No. XDB38000000), by the National Science Foundation of China (Nos 31771476 and 31930022), and by Shanghai Municipal Science and Technology Major Project (No. 2017SHZDZX01). S.Y.L. and K.A. are supported by JSPS KAKENHI (No. JP15H05707) and by AMED (No. JP20dm0307009). Y.-C.L. is supported by ONR (No. N00014-16-1-2828). H.F.M. is supported by the National Key R&D Program of China (No. 2018YFA0801100) and the National Natural Science Foundation of China (No. 11771010). J.K. is supported by the project RF Government Grant 075-15-2019-1885.

Author contributions

W.L. and L.N.C. conceived the idea; S.Y.L., H.F.M., W.L., K.A., and L.N.C. designed the research; S.Y.L., H.F.M., and W.L. performed the research; All authors, S.Y.L., H.F.M., J.K., Y.-C.L., W.L., K.A., and L.N.C., analyzed the data and wrote the paper.

Competing interests

The authors declare no competing interests.

Additional information

Supplementary information is available for this paper at <https://doi.org/10.1038/s41467-020-16238-0>.

Correspondence and requests for materials should be addressed to W.L., K.A. or L.C.

Peer review information *Nature Communications* thanks Aneta Stefanovska and the other, anonymous, reviewer(s) for their contribution to the peer review of this work. Peer reviewer reports are available.

Reprints and permission information is available at <http://www.nature.com/reprints>

Publisher's note Springer Nature remains neutral with regard to jurisdictional claims in published maps and institutional affiliations.

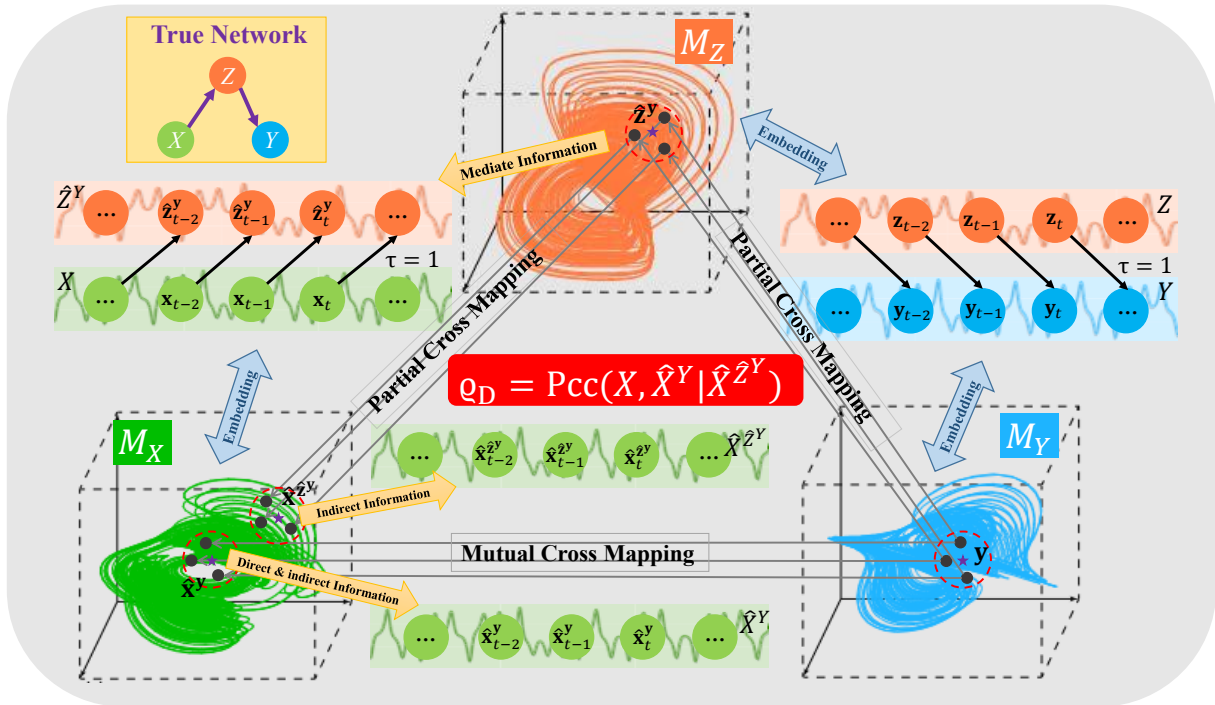


Open Access This article is licensed under a Creative Commons Attribution 4.0 International License, which permits use, sharing, adaptation, distribution and reproduction in any medium or format, as long as you give appropriate credit to the original author(s) and the source, provide a link to the Creative Commons license, and indicate if changes were made. The images or other third party material in this article are included in the article's Creative Commons license, unless indicated otherwise in a credit line to the material. If material is not included in the article's Creative Commons license and your intended use is not permitted by statutory regulation or exceeds the permitted use, you will need to obtain permission directly from the copyright holder. To view a copy of this license, visit <http://creativecommons.org/licenses/by/4.0/>.

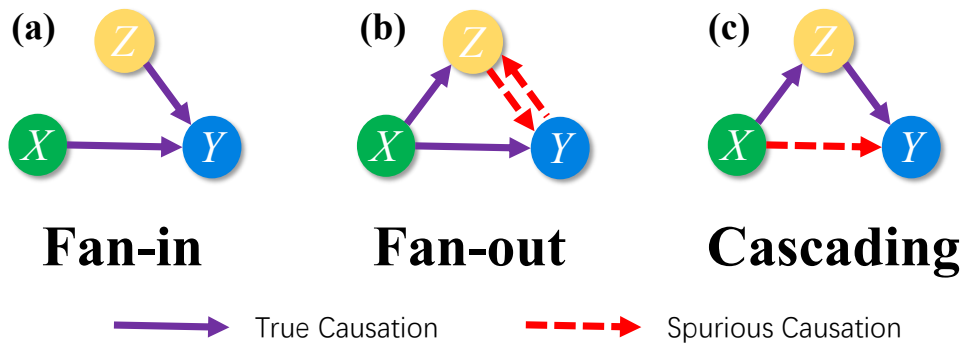
© The Author(s) 2020

Partial cross mapping eliminates indirect causal influences

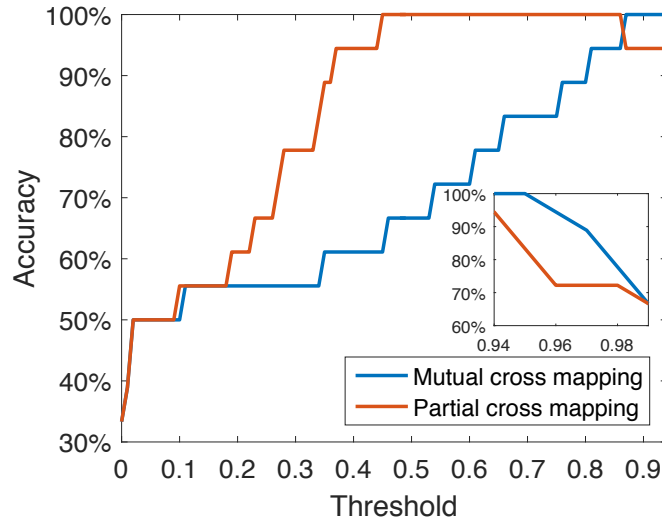
Leng et al.



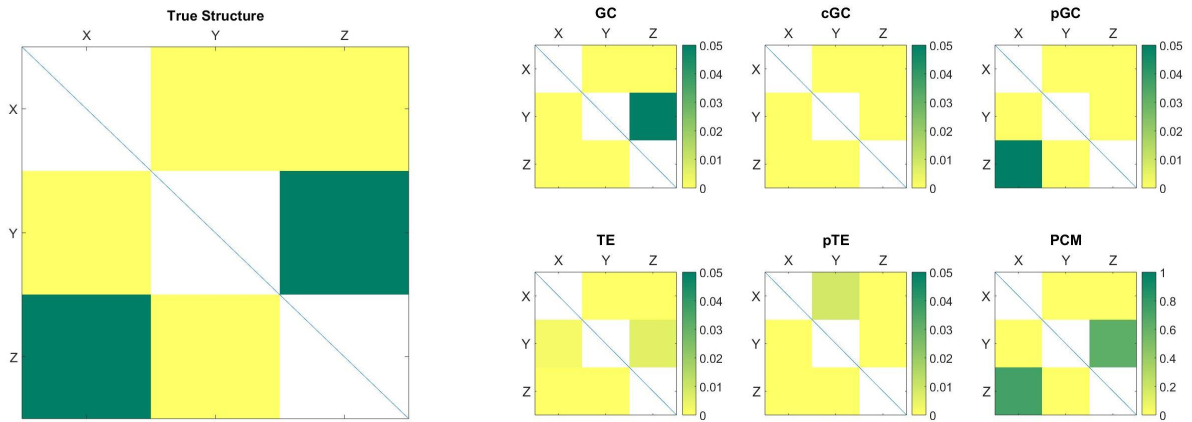
Supplementary Figure 1. A precise illustration for the PCM framework of the three variables interacting in a unidirectional causal chain. Here, the time delay of causal influence is set illustratively as 1. The indirect information is denoted by a successive estimating from M_Y to M_Z then to M_X (the slashed grey arrows labeled with Partial Cross Mapping) and the mapping from M_Y to M_X (the horizontal grey arrows labeled with Mutual Cross Mapping) contains both direct and indirect information. The partial correlation thus eliminates the indirect part. Here in each mapping procedure, an optimal time delay is searched to maximize the information transfer.



Supplementary Figure 2. Basic network motifs with causation detection. Large-scale networks possess a small set of recurring patterns, i.e., network motifs, which are the basic building blocks of any complex network. The red dashed arrows show spurious causation that easily to be wrongly detected by the existing methods.



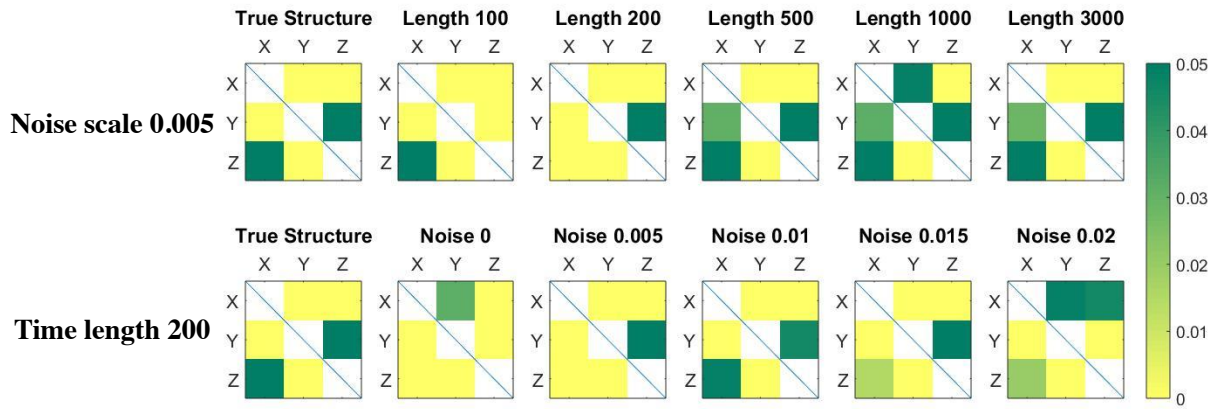
Supplementary Figure 3. Detection accuracy versus threshold T for the PCM and the MCM methods for the benchmark logistic model of three species in the main text. Shown are the accuracy with 18 indices (ϱ_D or ϱ_C) for all possible links in the three network structures listed in Figs. 1a-c of the main text. Notice that when $T = 0.5$, the MCM method not only misidentifies the indirect causal links, but also reaches wrong results in other links. When $0.95 > T > 0.85$, MCM could achieve 100% accuracy, however, it is not reasonable to choose such a high threshold value larger than 0.85 in practice. Notice that in this benchmark system, the index values (ϱ_C or ϱ_D) for a true positive direct causal link are of a rather high level, therefore the detection accuracy only decreases when the threshold is approaching 1 (see the partial enlarged view).



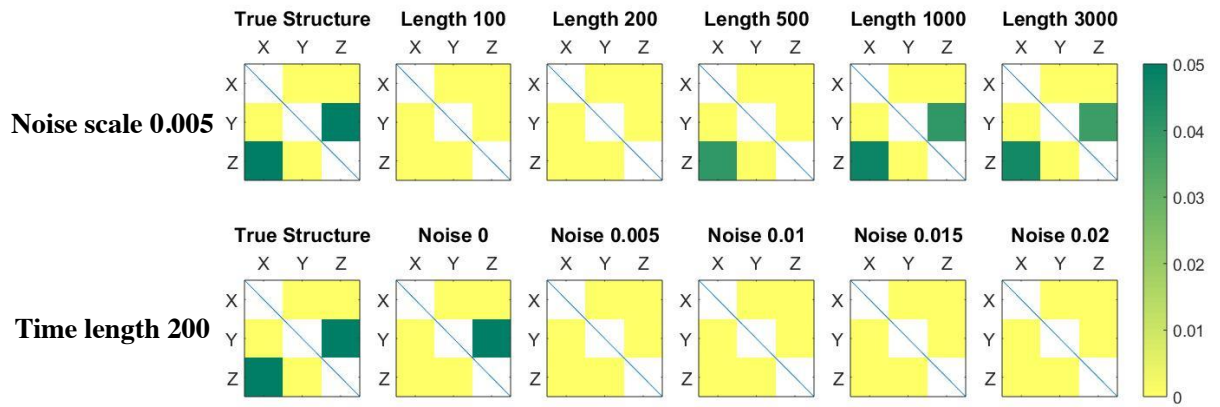
Time length 200 Noise scale 0.005

Supplementary Figure 4. Comparison results of the causation detection methods using a model of three species interacting in a chain mode. The true structure is shown by the left panel. The representative methods, including the GC, the cGC, the pGC, the TE, and the pTE, cannot identify the correct structures, while our method, the PCM, is able to identify the true causations correctly and completely. Here the denoted time lengths and the noise scales are relative to the real scale of the system.

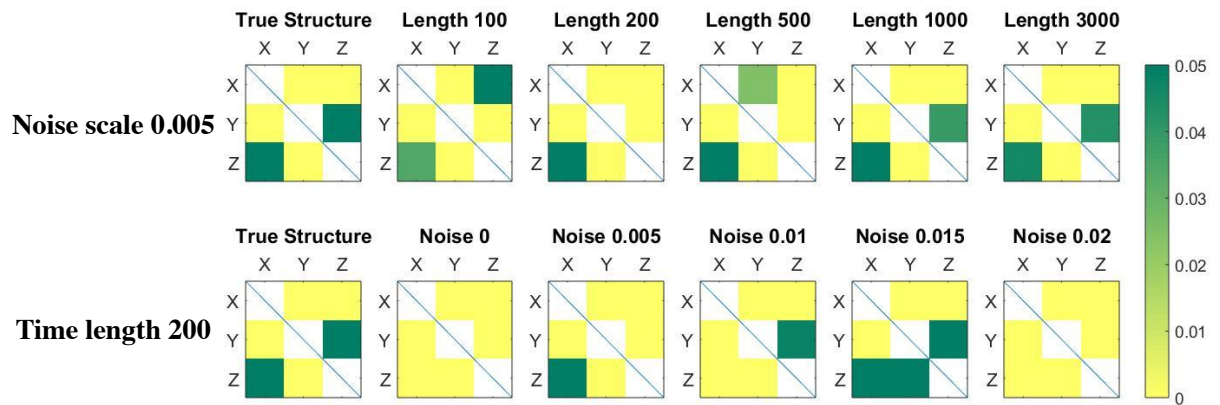
GC



cGC

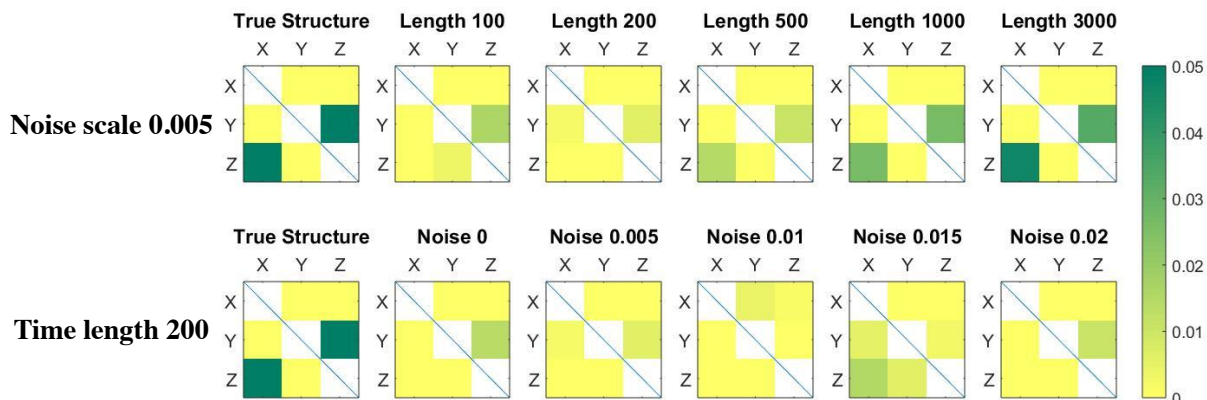


pGC

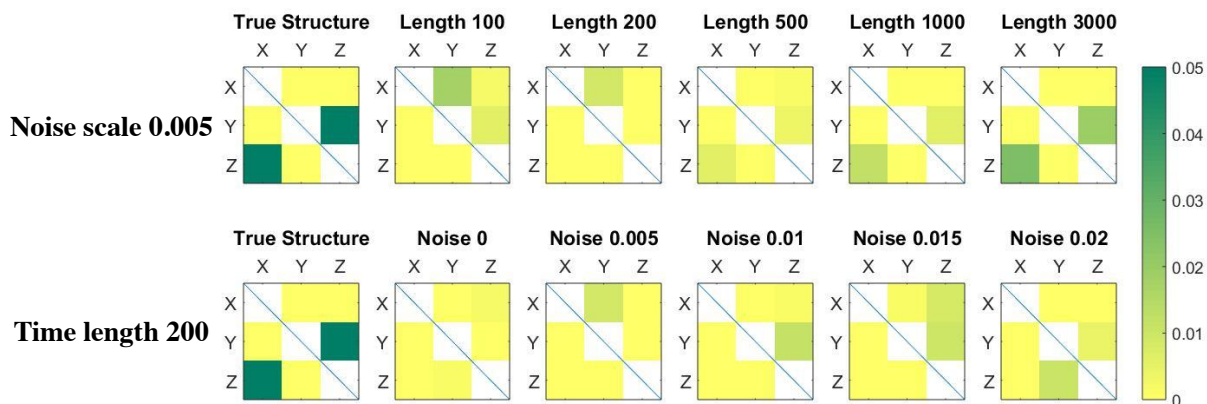


Supplementary Figure 5. Comparison results for causations detection by using the GC, the cGC, and the pGC. Here the denoted time lengths and the noise scales are relative to the real scale of the system.

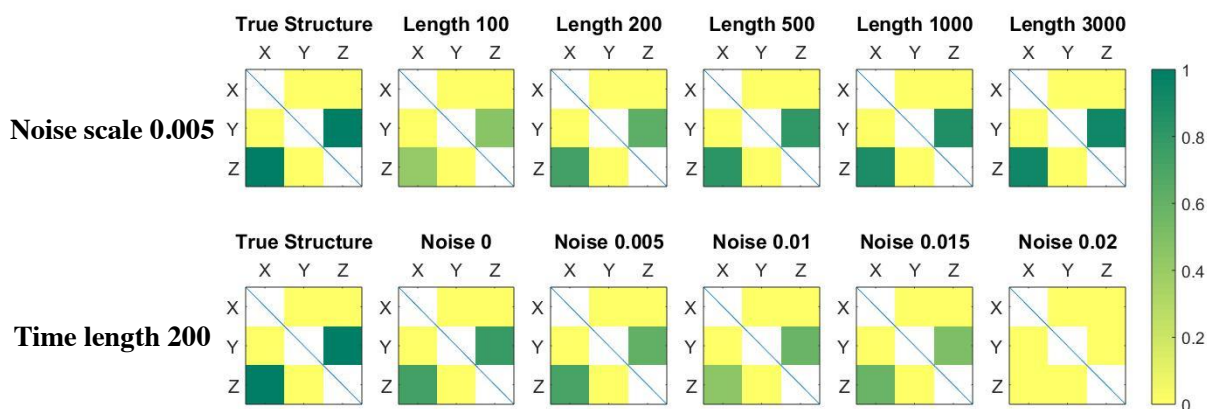
TE



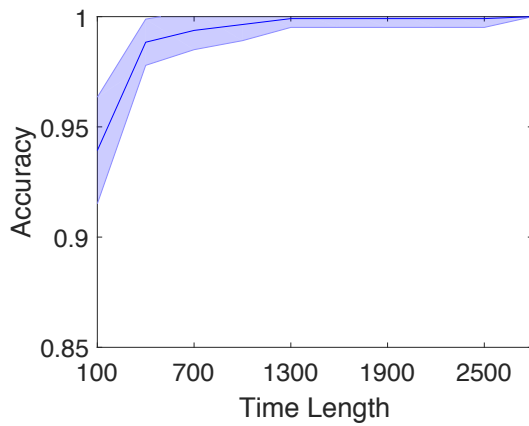
pTE



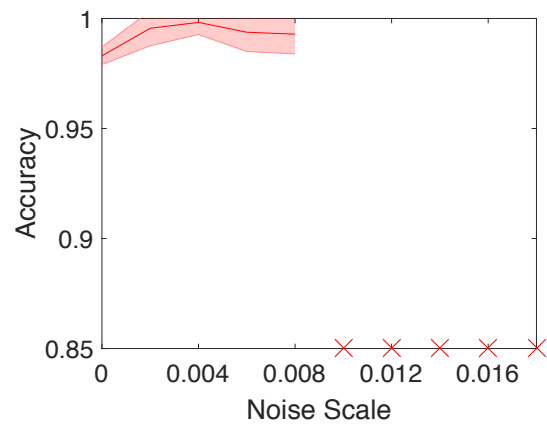
PCM



Supplementary Figure 6. Comparison results for causations detection by using the TE, the pTE, and the PCM. The PCM method outperforms all the other methods here and the methods in Supplementary Figure 5 as well. Here the denoted time lengths and the noise scales are relative to the real scale of the system.

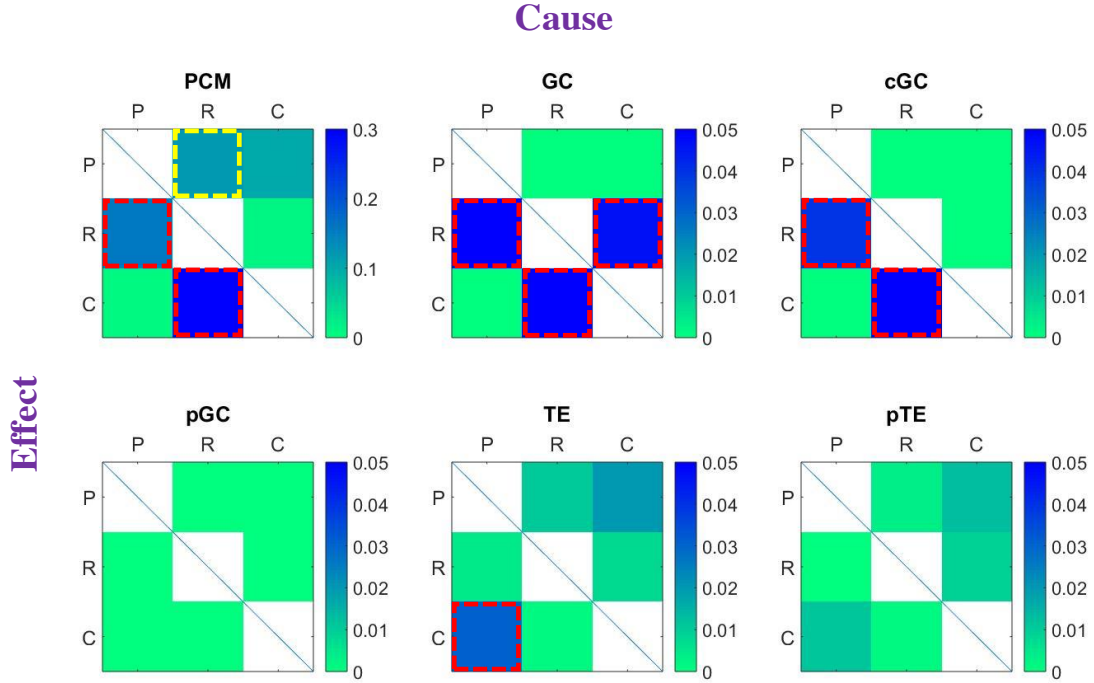


(a) Fixed noise scale 0.002.

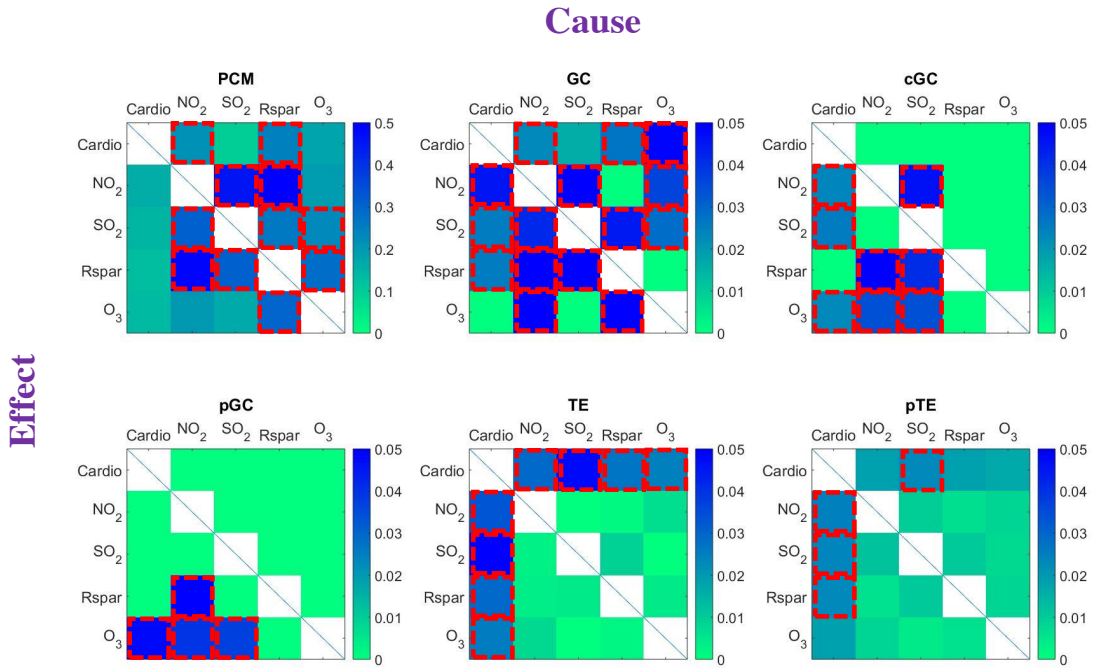


(b) Fixed time length 1000.

Supplementary Figure 7. Robustness tests of PCM against time series of different time lengths and noise scales with the networked system consisting of eight species in Supplementary Note 4. The shaded area represents the standard deviation of the PCM results of 100 simulations. The system becomes divergent when the noise scale exceeds 0.01 (shown by “x” on the horizontal axis). Here the time lengths denote the system’s absolute time unit and the noise scales are the ratio of the noise strength to the system’s amplitude. The threshold value is selected to be 0.5 in this analysis.

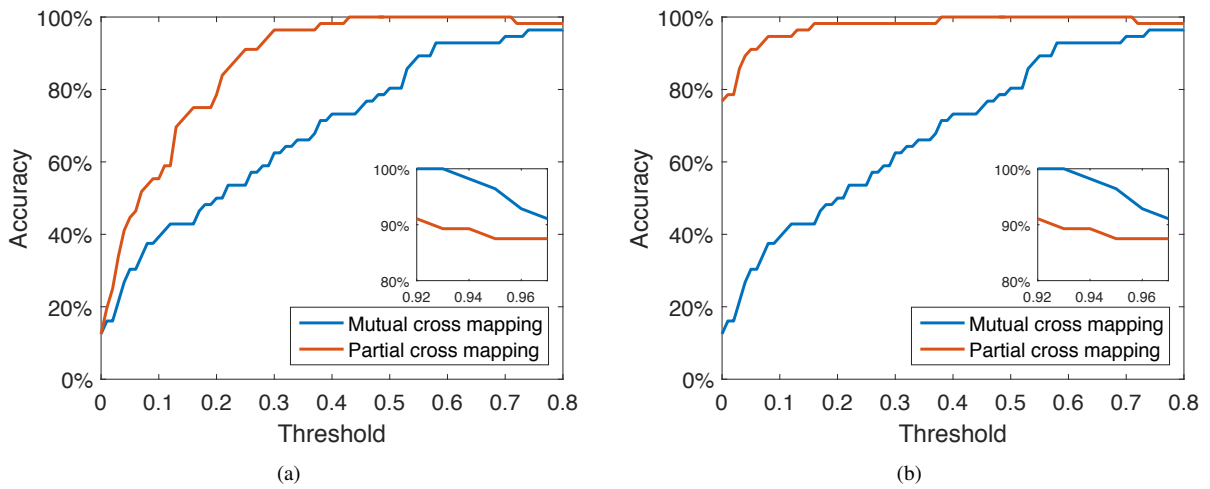


(a) Food chain network of three plankton species.

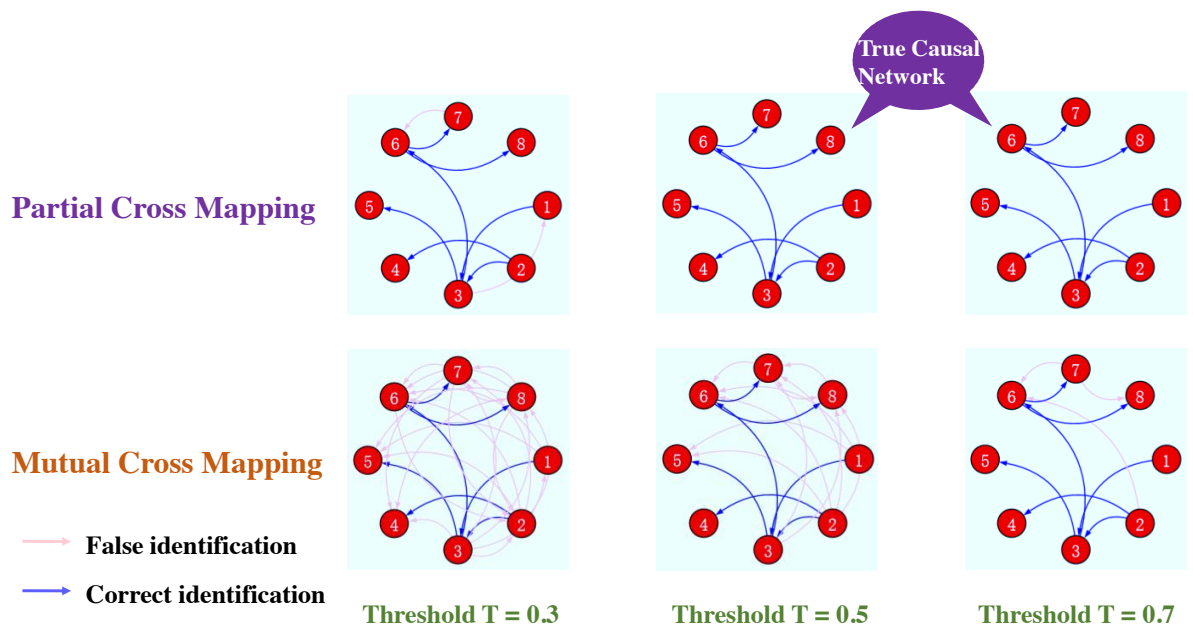


(b) Air pollutants and cardiovascular diseases.

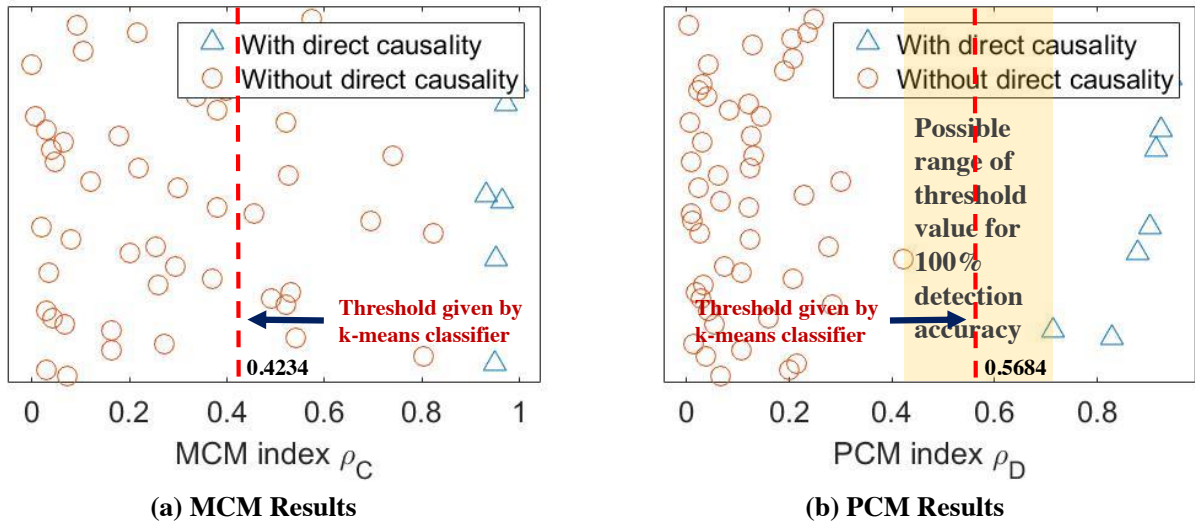
Supplementary Figure 8. Comparison results of causations detection methods with the representative real-world examples. Here, the regions highlighted by the dash boxes correspond to the detected causal links by the respective methods, and the names, *Cyclopooids*, *Rotifers*, and *Pico cyanobacteria*, are abbreviated as C, R, and P, respectively.



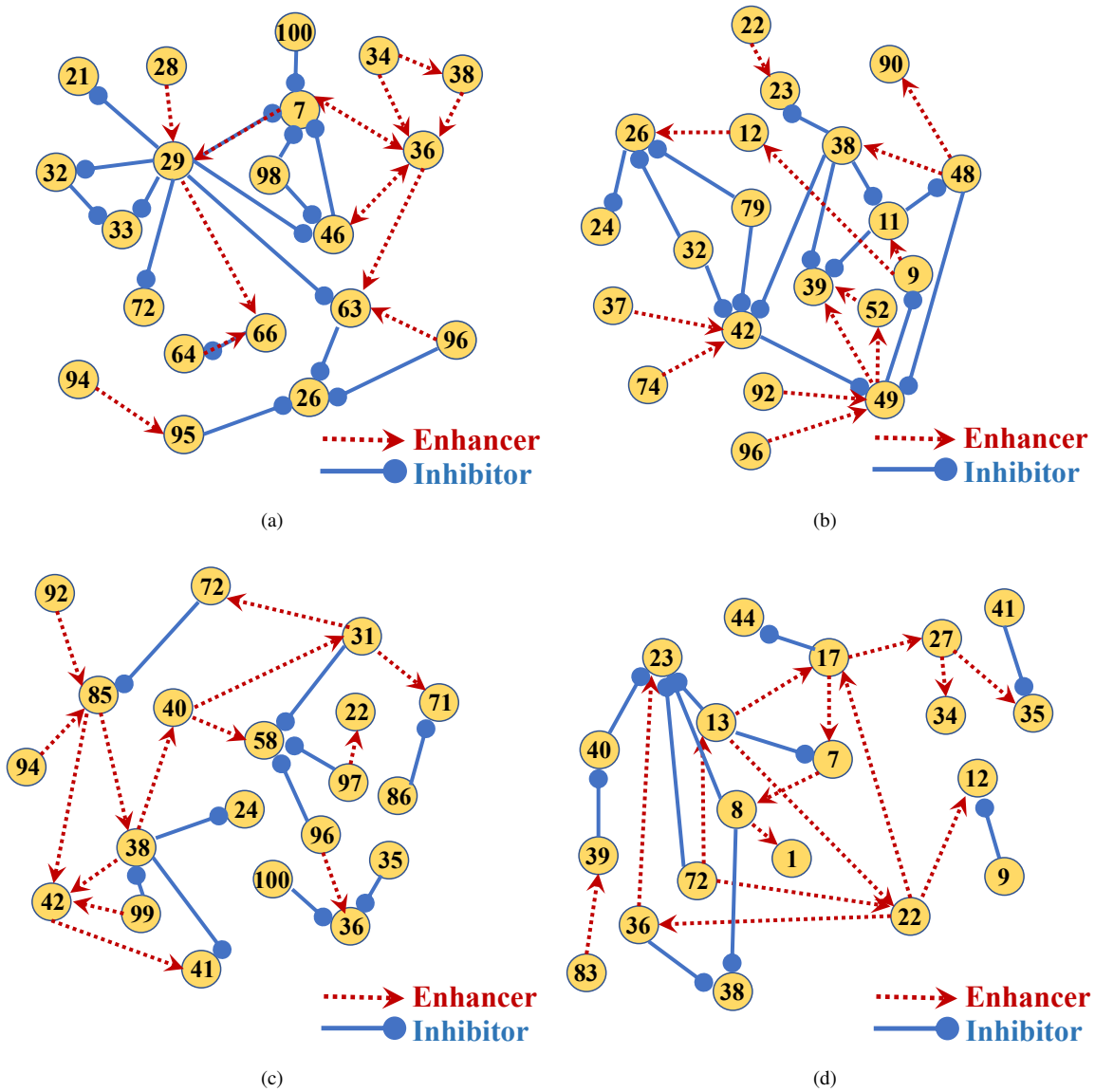
Supplementary Figure 9. Detection accuracy versus threshold T when the PCM and the MCM methods are in the logistic model Supplementary Equation (4) of eight interacting species. (a) No use of the accessory measure γ . (b) The accessory measure $\gamma \geq 70\%$ is used, which improves the detection accuracy ($\geq 80\%$) for the PCM method for small values of T . The partial enlarged views show that the accuracy decreases when the threshold is too large.



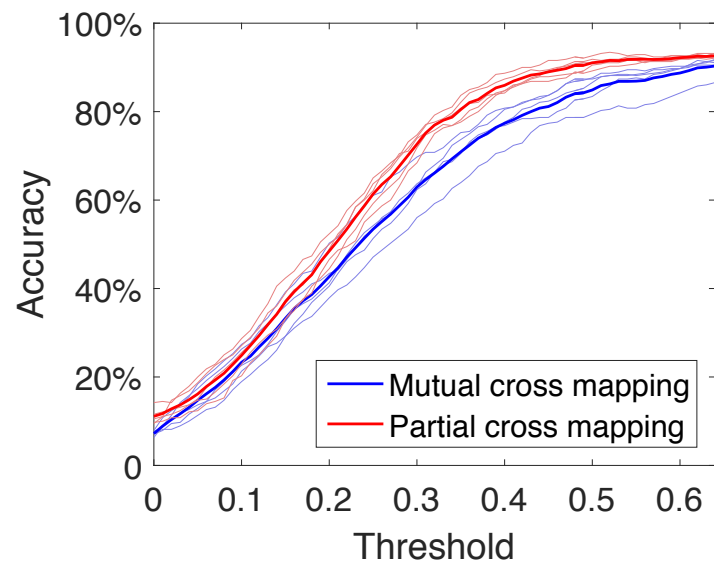
Supplementary Figure 10. Using the PCM and the MCM methods to reconstruct the causal networks, respectively, with different values of T for model Supplementary Equation (4). The blue and pink arrows indicate the correctly and falsely detected direct causal links, respectively.



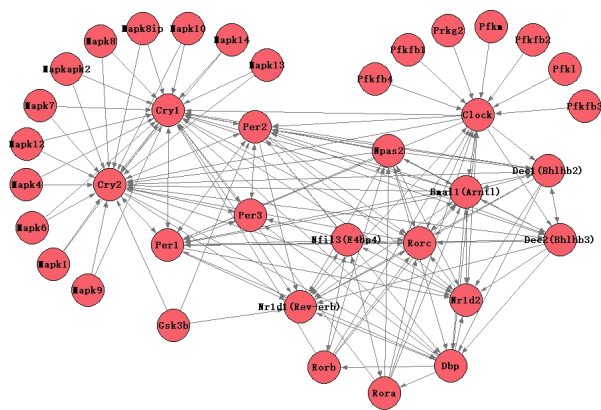
Supplementary Figure 11. Threshold value selected by k-means classifier for the eight species model. (a) The threshold value induced from k-means classifier is ineffective which produces a lot of false positives for MCM results. (b) For PCM results, the two groups with and without direct causality are distinguished from each other but are concentrated within the interior. This fact facilitates the practical selection of the threshold value and improves the robustness of the PCM method.



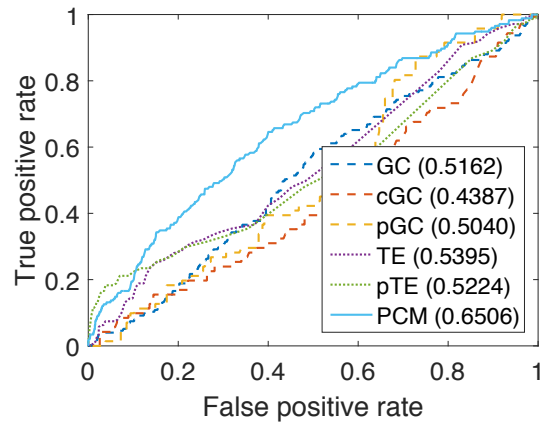
Supplementary Figure 12. Four gene regulatory networks. The four networks together with the one described in the main text [Fig. 4a], with which the PCM and the MCM methods are tested, respectively, in Supplementary Figure 13.



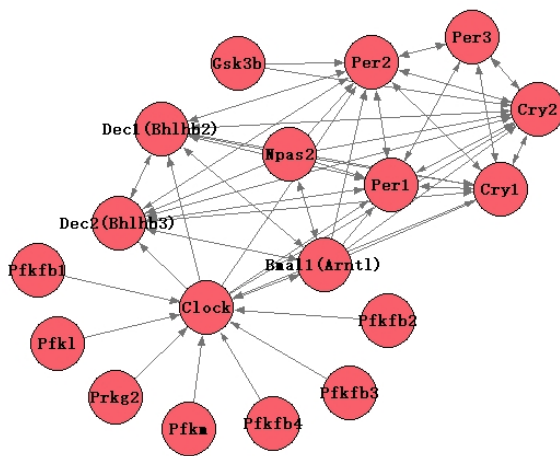
Supplementary Figure 13. Detection accuracy versus the threshold T by using the PCM and the MCM methods for the five gene regulatory networks. The red (blue, resp.) thick curve corresponds to an average detection accuracy of the red (blue, resp.) thin curves, for the five gene regulatory networks by using the PCM (MCM, resp.) method.



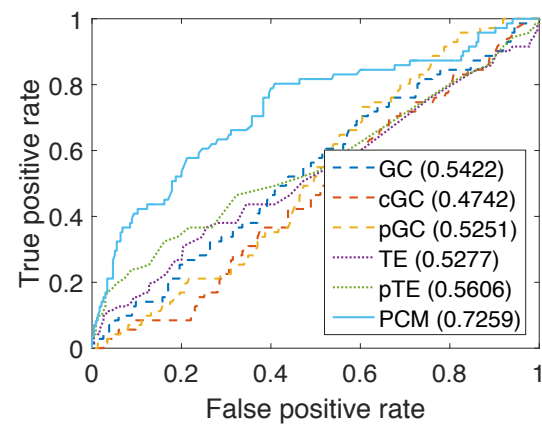
(a)



(b)

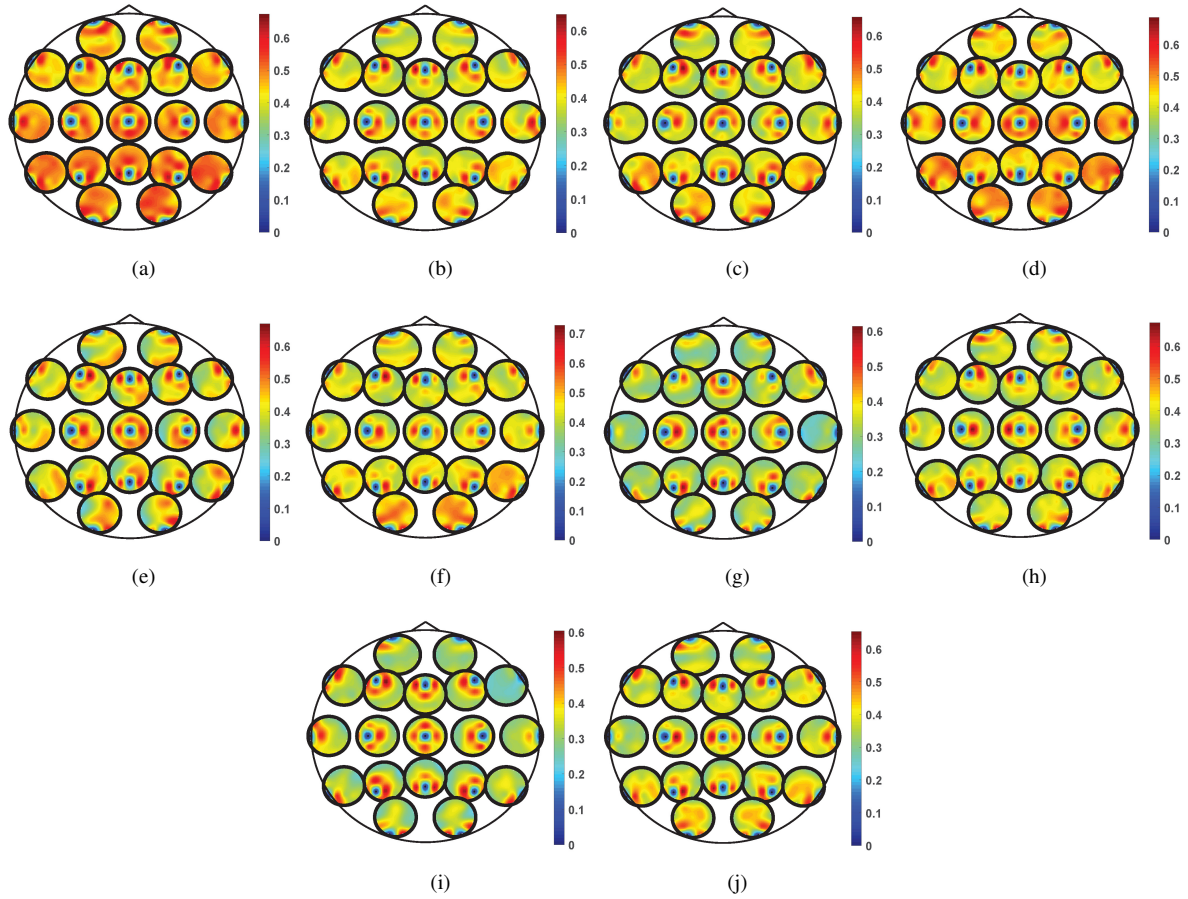


(c)

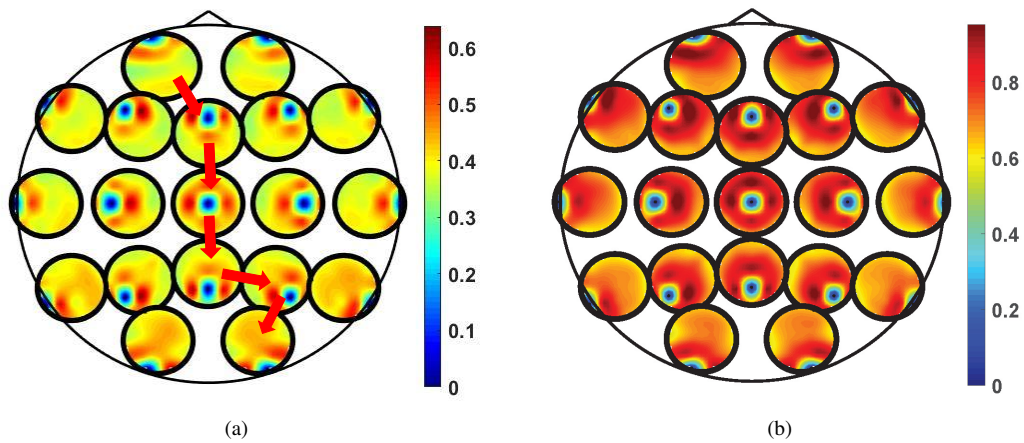


(d)

Supplementary Figure 14. Comparison results on causations detection in the real gene regulatory networks containing key genes of circadian rhythms by using different methods. Here, two sub-functional regulatory gene networks with 37 (a) and 18 (c) genes are analyzed, respectively. The PCM method outperforms the other methods in the analyses of the both networks [(b) and (d)]. The phase space reconstruction parameters are taken as $E = 2$ and $\tau = 1$, and the networks are plotted by the software Pajek (<http://mrvar.fdv.uni-lj.si/pajek/>).

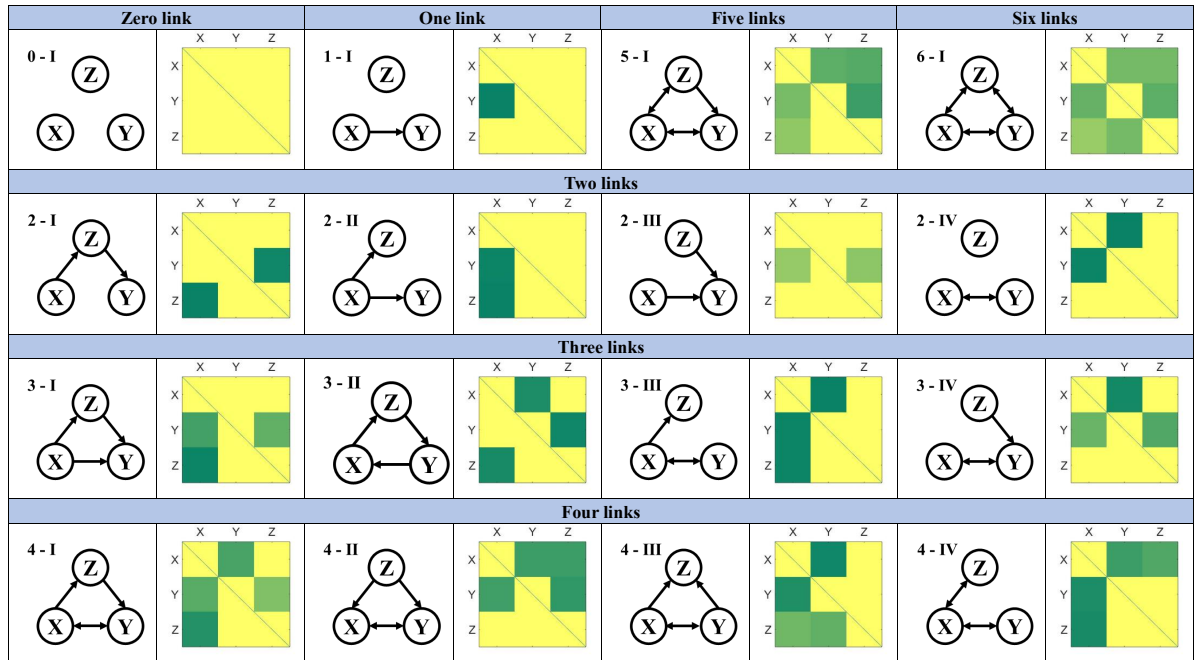


Supplementary Figure 15. The results by using the PCM method on the EEG recordings data for the 10 subjects, respectively. Here, each figure corresponds to an average over 10 randomly selected blocks during which the recording is a continuous measurement that is cleaned of apparent artefacts. In particular, the small circles are positioned at the approximate location of the corresponding electrode placed on the skull. The causation measures from one electrode channel to all the others are displayed at the same relative position within the small circle. The plotting scheme is adapted from [1]. The phase space reconstruction parameters are taken as $E = 6$ and $\tau = 6$.



Supplementary Figure 16. Using the PCM method reveals direct electrical information pathways in the human brain. Here, (a) the PCM and (b) the MCM measures are shown between all the possible pairs of 19 channels of the EEG recordings, averaged over 10 subjects and 10 randomly-selected blocks. The detection result using the PCM method is able to reveal the information pathways [e.g., a sample pathway is highlighted by the red arrows in (a)], while the MCM method produces very dense network in every small circle in (b), which indicates the information transmitting in almost every direction but no pathway of specific function.

Supplementary Table 1. Using the PCM method to detect causations for all the possible types of interacting structures of three species. Here, the detecting results are shown, respectively, in the colored matrices, where the direction of each causal interaction is from the variable in the column of the matrix to the different variable in the row. In generating the data of time series, the initial values are taken randomly from the interval $[0, 1]$. The parameters of the phase space reconstruction are taken as: $E = 4$ and $\tau = 1$.



Supplementary Table 2. Measures of all possible causal directions and the corresponding p -values. The system is the benchmark model of three interacting species in the three modes shown in Figs. 1a-c of the main text. The values in bold are the detections for $T \geq 0.5$ ($p \simeq 0$).

Directions	$X \rightarrow Y$	$Y \rightarrow X$	$X \rightarrow Z$	$Z \rightarrow X$	$Y \rightarrow Z$	$Z \rightarrow Y$
MCM in Fig. 1a	0.9847 (\checkmark)	0.3493	0.0140	0.0134	6.0100e-04	0.1035
PCM in Fig. 1a	0.9817 (\checkmark)	0.3322	0.0137	0.0175	0.0032	0.0961
p -values for PCM	0 (\checkmark)	6.9751e-26	0.6727	0.5910	0.9211	0.0031
MCM in Fig. 1b	0.8681 (\times)	0.4501	0.9846 (\checkmark)	0.6565 (\times)	0.5307 (\times)	0.9746 (\checkmark)
PCM in Fig. 1b	0.1871	0.2262	0.9573 (\checkmark)	0.3479	0.3662	0.9499 (\checkmark)
p -values for PCM	6.3838e-09	1.7688e-12	0 (\checkmark)	2.1943e-28	1.7027e-31	0 (\checkmark)
MCM in Fig. 1c	0.8052 (\times)	0.9674 (\checkmark)	0.9718 (\checkmark)	0.6005 (\times)	0.7576 (\times)	0.9593 (\checkmark)
PCM in Fig. 1c	0.4467	0.9590 (\checkmark)	0.8609 (\checkmark)	0.2725	0.2685	0.9480 (\checkmark)
p -values for PCM	9.7651e-48	0 (\checkmark)	3.8035e - 280 (\checkmark)	1.2785e-17	3.9153e-17	0 (\checkmark)

Supplementary Table 3. The scope of the GC-based, TE-based and PCM causation detection methods. The abbreviations could be find in Supplementary Note 3.

	Separable system	Non-separable system
Pairwise	GC, cGC, pGC, TE, pTE	MCM, PCM
Network	cGC, pGC, pTE	PCM

Supplementary Table 4. For the PCM method, the p -values associated with the seven detected direct causal links for the logistic model of the eight interacting species. Here, all the p -values for the true links are approximately zero, showing high statistical significance and accurate detection results as the PCM method is used.

Directions	$1 \rightarrow 3$	$2 \rightarrow 3$	$2 \rightarrow 4$	$3 \rightarrow 5$	$3 \rightarrow 6$	$6 \rightarrow 7$	$6 \rightarrow 8$
p -values	0	9.8212e - 148	0	0	1.7441e - 306	0	8.2680e - 240

Supplementary Table 5. For the food chain network of three plankton species, the p -values associated with all possible causal directions. The names of *Cyclopooids*, *Rotifers*, and *Pico cyanobacteria* are abbreviated as C, R, and P, respectively. The values in bold are the detections for $T \geq 10^{-1}$ ($p < 0.0016$).

Directions	C \rightarrow R	R \rightarrow C	C \rightarrow P	P \rightarrow C	R \rightarrow P	P \rightarrow R
p -values	0.7495	1.1302e - 17	0.0054	0.8259	0.0011	1.2119e - 05

Supplementary Table 6. PCM generated p -values for all possible causal directions between the air pollutants and the admission numbers of cardiovascular diseases in major hospitals in Hong Kong. The values in bold are the detections for $p < 10^{-9}$.

Directions	Cardio \rightarrow NO ₂	NO ₂ \rightarrow Cardio	Cardio \rightarrow SO ₂	SO ₂ \rightarrow Cardio
p -values	1.1268e-06	4.0209e - 11	2.0593e-05	0.0038
Directions	Cardio \rightarrow Rspar	Rspar \rightarrow Cardio	Cardio \rightarrow O ₃	O ₃ \rightarrow Cardio
p -values	8.7456e-05	3.3594e - 14	5.0206e-05	6.7548e-08
Directions	NO ₂ \rightarrow SO ₂	SO ₂ \rightarrow NO ₂	NO ₂ \rightarrow Rspar	Rspar \rightarrow NO ₂
p -values	8.6071e - 21	6.8415e - 47	6.5167e - 55	4.0150e - 63
Directions	NO ₂ \rightarrow O ₃	O ₃ \rightarrow NO ₂	SO ₂ \rightarrow Rspar	Rspar \rightarrow SO ₂
p -values	2.8376e-09	6.9308e-09	3.3639e - 21	8.1370e - 16
Directions	SO ₂ \rightarrow O ₃	O ₃ \rightarrow SO ₂	Rspar \rightarrow O ₃	O ₃ \rightarrow Rspar
p -values	2.3718e-07	1.7075e - 12	2.6498e - 20	2.0512e - 18

Supplementary Note 1. Detecting causations in all types of structures for three interacting species

In addition to the three interacting structures for three species in the main text, our proposed PCM method is effectively applicable to detecting causations for all the other types of interacting structures as listed in Supplementary Table 1. Particularly, as is well-known, the structures, such as the fan-out spurious causation due to the common source [Supplementary Table 1 #2-II and Supplementary Figure 2(b)] and the indirect spurious causation due to the cascading [Supplementary Table 1 #2-I and Supplementary Figure 2(c)], always result in false detections when the existing methods are used. However, our PCM can achieve in distinguishing these spurious links. Additionally, these two spurious links, with the fan-in mode [Supplementary Table 1 #2-III and Supplementary Figure 2(a)], become the elementary structures for building blocks in any complex networks [2, 3]. Since the PCM method can achieve accurate detections of causations in these elementary modes, using the PCM method to reconstruct causal networks of large scale becomes doable and reliable.

In our systematic analyses, the species dynamics of X , Y , and Z are taken as the logistic maps with unchanged parameters for all the possible interacting structures. More precisely, the model of the interacting species is:

$$x_t = x_{t-1}(\alpha_x - \alpha_x x_{t-1} - \beta_{xy} y_{t-1} - \beta_{xz} z_{t-1}) + \epsilon_{x,t-1}, \quad (1)$$

$$y_t = y_{t-1}(\alpha_y - \alpha_y y_{t-1} - \beta_{yx} x_{t-1} - \beta_{yz} z_{t-1}) + \epsilon_{y,t-1}, \quad (2)$$

$$z_t = z_{t-1}(\alpha_z - \alpha_z z_{t-1} - \beta_{zx} x_{t-1} - \beta_{zy} y_{t-1}) + \epsilon_{z,t-1} \quad (3)$$

with the parameters that are set, respectively, as $\alpha_x = 3.7$, $\alpha_y = 3.78$, and $\alpha_z = 3.72$. The coupling strength are taken as 0.35 or 0 to form the corresponding structure. The last term $\epsilon_{i,t}$ ($i \in \{x, y, z\}$) in the above equations are the white noise with the strength 0.005 (see Supplementary Note 3 for detailed information on the scale of the noise). We consider 100 trails with the length of 1000 points, which are randomly selected from the generated time series with the length of 5000 points. Here, the sampling rate is 1 Hz, so the number of time points matches exactly the time unit of the system. The average of the PCM index for each possible causal direction over these 100 trails is shown in Supplementary Table 1.

Supplementary Note 2. Additional information for benchmark systems in the main text

As described in the main text, the value of the threshold T is set to be 0.5. The PCM method reconstructs correctly the causal networks of different structure for the benchmark system. How does the choice of the threshold T affect the detection accuracy for PCM or the previous MCM method? For the benchmark systems in main text [Fig. 3], we show in Supplementary Figure 3, for both methods, the detection accuracy varies as the threshold value is increased. Here detection accuracy denotes total correct classification rate (both negative and positive) of direct causal links. However, the range of T values in which the detection accuracy approaches 100% is much broader for PCM than for MCM, demonstrating the robustness and broad applicability of the PCM method to real-world systems when *a priori* knowledge for prescribing the value of T is lacking.

For data integrity and statistical significance, we list in Supplementary Table 2 all the computational results for all the possible causal directions for the three modes in Figs. 1a-1c [or Fig. 3a] in the main text. Also listed in this table are the results on the corresponding p -values for the PCM measures, where the p -values are obtained by testing the hypothesis of no partial correlation against the alternative that there is non-zero partial correlation. The final results are all verified by multi-testing corrections via the Bonferroni adjustment ($p < \alpha/n$), where n is the number of the edges in the network [4, 5].

Supplementary Note 3. Systematic comparison of the PCM method with the representative methods

Presently, there are three major paradigms for identifying and quantifying causal interactions: the celebrated Granger causality, the entropy based methods, and the mutual cross mapping. The Granger causality and the entropy based methods are likely to work ineffectively in the situation where the relevant dynamical variables are

non-separable. As a matter of fact, in the benchmark and real-world nonlinear dynamical systems, which are also the systems we are mainly investigating in this work, the non-separable variables are dominantly present. The mutual cross mapping based methods allow for detecting causations between the non-separable variables but cannot distinguish direct causation from indirect ones (as described and compared in the main text). Here, we perform systematic comparison studies on the performances of the representative methods in the literature and our PCM method using the benchmark systems and the real-world examples. The scope of the methods investigated here are summarized in Supplementary Table 3.

3.1. Benchmark systems with different time lengths and different noise scales

We still use the coupled logistic maps Supplementary Equations (1)-(3) as a benchmark system to perform the comparison study. We consider the causal chain mode $X \rightarrow Z \rightarrow Y$ where $\beta_{yz} = 0.1$, $\beta_{zx} = 0.1$, and the other coupling parameters are set as zero. Different lengths of time series (i.e., 100, 200, 500, 1000, 3000) and different noise levels (i.e., 0, 0.005, 0.01, 0.015, 0.02) are, respectively, taken into account. Here, the sampling rate is 1 Hz, so the number of time points matches exactly the time unit of the system. We will use the term “time length” to denote the absolute length of the time duration for a time series. Additionally, we generate the white noises with respect to each time unit and use the term “noise scale” as the ratio between the noise strength and the amplitude of the system dynamics (e.g., the amplitude is 1 for the logistic map, so the noise strength is exactly the same as the noise scale here). We compute the causation index for all the six possible causation directions by using the following methods, respectively: the Granger causality (GC), the conditional Granger causality (cGC), the partial Granger causality (pGC), the transfer entropy (TE), the partial transfer entropy (pTE), and our method, the PCM. The realization details for all the methods, the significance test methods, and the other numerical configurations are summarized in Supplementary Note 5.

We first compare the six methods using the time series with the time length of 200 and with the noise scale 0.005 as well. As shown in Supplementary Figure 4, only the proposed PCM method is able to identify the correct causation structure of the unidirectional chain, while the other methods are all failed in finding the correct structure.

Next, we test the above-mentioned methods with different time lengths and different noise scales. We then illustrate the range of application for each method in details. For the original GC, the detection results are quite unstable [Supplementary Figure 5], which is due to the non-separable variables are present in our nonlinear system. As a matter of fact, the Granger causality method and its extensions (the cGC and the pGC), which are all based on regression, are theoretically unsuitable for causation detection for nonlinear systems with non-separable variables. Although the conditional and the partial Granger causality tests perform well only when the time length is sufficiently long, the detection results are not based on the solid ground. This is because the regression actually produces a tremendously large deviation from the true dynamics in the first step of the GC detection where a presumed regression model is required to fit with the observed time series. Such a fitting deviation definitely renders the results obtained by the GC method unreliable. As for the data produced by a presumed model with strong stochasticity, the GC as well as its extensions is still regarded as the most useful technique in causation detections. However, as for the data produced by any unknown dynamical model with weak and moderate stochasticity, our PCM method is more reliable and effective due to its solid ground of dynamical systems theory.

The TE method was developed to deal with both linear and nonlinear systems. For the special case of the Gaussian variables, the GC and the TE are in fact equivalent to each other [6]. However, the TE and the pTE methods require reconstruction of the probability distributions of the pertinent variables from the observed data. The performance of causation detections by using these two method thus significantly depend on the time length of the available time series, as shown in Supplementary Figure 6. Moreover, it is emphasized that, theoretically, neither the TE nor the pTE allow for any non-separate variables in causation detections.

However, for our proposed PCM method, we could easily find that PCM indeed outperforms the other representative frameworks of causation detections. PCM is not restricted by the separability condition and effective even when the time length is not sufficiently long. However, the PCM is sensitive to large noise, and will produce false negative detections which is inevitable.

To further explore the robustness of the PCM framework against time series lengths and the noise scales, we performed an additional numerical analysis using the eight species system introduced in Supplementary Note 4. As expected, Supplementary Figure 7 shows that the detection accuracy increases with the time length of the time series used in simulations but always remains at a high level, confirming the effectiveness of our PCM framework in dealing with an extremely small amount of data. In addition, increasing the noise scale only slightly lowers the

detection accuracy. Note that the system becomes divergent as the noise scale is larger than 0.01 [shown by “×” on the horizontal axis in Supplementary Figure 7(b)]. These also demonstrate that our PCM framework is useful when the noisy perturbation is introduced in a manner of small or moderate intensity.

3.2. Comparison on real-world examples

We will compare our PCM method with other causal assessment methods also on the real-world examples. Here we perform the comparison with the three plankton species food chain network and the example of air pollution with cardiovascular diseases.

As shown in Supplementary Figure 8, the GC and cGC could successfully identify the chain structure among the three species, but fail to detect the weak causation from *Rotifers* to *Pico cyanobacteria*. However, GC even produces a false link from *Cyclopooids* to *Rotifers*, which shows GC is unsuitable for detecting causality in this system. Moreover, pGC, TE and pTE can hardly detect the structure and even produce false positive. As to the second example, methods except PCM all find causal links from cardiovascular diseases to the air pollutants, which is unreasonable to the true network. And cGC and pGC fail to find any causal relation from air pollutants to cardiovascular diseases, which has been proved in literature [7, 8].

3.3. Comparison of PCM and DBI

First, the method of the dynamical Bayesian inference (DBI) does not require the detailed knowledge of the explicit equations in the models but only uses a delicate selection of a basis set in some function space for data regression [9, 10, 11, 12]. It is applicable for general autonomous and nonautonomous systems. Our PCM framework is a model-free method, only based on the embedding theorem, which is theoretically suitable for dealing with autonomous systems or/and nonautonomous systems with some particular forms as mentioned in the main text. More concretely, the PCM framework works for the switching systems where the switching points can be located and each duration between the consecutive switching points is sufficiently long, while the DBI is applicable for more types of nonautonomous systems, including the dynamical oscillators with time-evolving coupled functions or/and with various types of noise [9]. Second, the DBI method can infer the exact coupling functions and underlying dynamical mechanisms, while our PCM framework focuses much on the detection of causal relations. So, the connections detected by the DBI could be regarded as effective connectivity while the causal relations found by the PCM framework are more like functional connectivity [13]. Additionally, our PCM is able to distinguish direct causations from indirect ones, while the DBI method could be further extended to a conditional version. Both methods have their own particular advantages and could be used in a complementary manner. For example, in highly complex networks, our PCM framework can first detect the basic network structures based on the observed data, significantly simplifying initial regression structure with the function basis set.

Supplementary Note 4. Reconstruction of direct causal networks of eight benchmark species

We consider the system

$$\begin{aligned}
x_1(t) &= x_1(t-1)[3.9 - 3.9x_1(t-1)] + \epsilon_{1,t}, \\
x_2(t) &= x_2(t-1)[3.5 - 3.5x_2(t-1)] + \epsilon_{2,t}, \\
x_3(t) &= x_3(t-1)[3.62 - 3.62x_3(t-1) - 0.35x_1(t-1) - 0.35x_2(t-1)] + \epsilon_{3,t}, \\
x_4(t) &= x_4(t-1)[3.75 - 3.75x_4(t-1) - 0.35x_2(t-1)] + \epsilon_{4,t}, \\
x_5(t) &= x_5(t-1)[3.65 - 3.65x_5(t-1) - 0.35x_3(t-1)] + \epsilon_{5,t}, \\
x_6(t) &= x_6(t-1)[3.72 - 3.72x_6(t-1) - 0.35x_3(t-1)] + \epsilon_{6,t}, \\
x_7(t) &= x_7(t-1)[3.57 - 3.57x_7(t-1) - 0.35x_6(t-1)] + \epsilon_{7,t}, \\
x_8(t) &= x_8(t-1)[3.68 - 3.68x_8(t-1) - 0.35x_6(t-1)] + \epsilon_{8,t},
\end{aligned} \tag{4}$$

where $\epsilon_{i,t}$ ($i = 1, \dots, 8$) terms are white noise of zero mean and standard deviation 0.005 (see Supplementary Note 3 for detailed information on the scale of the noise). Supplementary Figure 9 shows the detection accuracy versus the threshold T for both the PCM and MCM methods. The PCM method gives much better performance in

reconstructing the direct causal networks. The accessory measure γ introduced in the main text is also shown in Supplementary Figure 9. Taking γ into account can improve the detection accuracy for small values of T .

Supplementary Figure 10 presents the reconstructed direct causal networks for three different values of T : $T = 0.3$, $T = 0.5$, and $T = 0.7$. We see that, even for $T = 0.3$, the PCM method recovers almost all the direct causal links, and for $T = 0.5$ and $T = 0.7$, the reconstruction error is essentially zero. In contrast, the MCM method gives dense networks containing many indirect causal links and false direct links even for T above 0.5. Supplementary Table 4 lists the p -values verified by the multi-testing corrections for the seven direct causal links.

It is worthwhile to mention that using the PCM method with a larger value of T does not always result in the most accurate detection of causations not only for the data that are generated by dynamical models (see Supplementary Figures 3 & 9) but particularly for the real-world data where the internal or external perturbations are unavoidable. The PCM measurement that we design actually quantifies the association between the variables whose interacting structure is even nonlinear. Such a nonlinear interaction, together with computation of normal/partial correlation and various types of perturbations, are likely to reduce to some extent the absolute value of our measurement, which makes the selection of a larger value of T impractical for causations detection in real applications. Therefore, the results in Supplementary Figure 10 manifest that the PCM method does not require the use of a larger value of T , more applicable to applications. The effective selection of threshold value is also much more realizable and robust for our PCM method than for MCM method, see Supplementary Note 5 and Supplementary Figure 11.

Supplementary Note 5. Quick tips for parameter selections, significance tests, and numerical configurations

Q1. How to determine computationally the embedding dimensions and time lags in the phase space reconstruction?

A1. A theoretical requirement guaranteeing the topological equivalency between reconstructed manifold and the original attractor is that the embedding dimension is twice larger than the fractal dimension of the attractor. In practice, we use the method of false nearest neighbor (FNN) and delayed mutual information (DMI) to determine the embedding dimensions and time lags respectively. Moreover, method of linear autocorrelation or other advanced techniques can also be applied in determining these parameters [14, 7]. In the EEG example in Supplementary Note 7, the embedding parameters are adapted from [15]. All these parameters are listed in the captions of the corresponding figures.

Q2. How many nearest neighbors are used in the mutual cross mapping procedure?

A2. We use $E + 1$ nearest neighbors (E is the embedding dimension), which is the minimum number of points needed for a bounded simplex in an E -dimensional space.

Q3. How to determine the threshold value T in practice?

A3. The selection of the threshold is indeed to some extent empirical. In this research, we provide robustness tests on the detection accuracy versus different threshold levels, which shows a practically effective threshold value really exists in a rather wide range (refer to Supplementary Figures 3, 9, 10, 13). Moreover, we additionally provide possible methods regarding the selection of threshold in practice. Unsupervised classifiers such as k-means clustering [16] could be applied to determine the threshold value by classifying the detection results into two groups (i.e., with or without direct causation). And the t-test could also be performed to determine the significance level of the difference between pairs of nodes with or without direct causal relation, while a low p -value represents the two groups are distinguished from each other but concentrated within the interior, thus the selection of a threshold is indeed realizable. As an example, we show in Supplementary Figure 11 the threshold values selected by k-means clustering for classification method for the MCM and PCM detection results of the eight species model discussed in Supplementary Note 4, where results for all possible causal directions are denoted. For the MCM results, though the true positive direct causal links have relatively higher index values, it is difficult to clearly distinguish the two groups with or without direct causality, and the threshold value induced from k-means classifier is ineffective which produces a lot of false positives. However, our PCM method successfully eliminates indirect causation with a distinguishable difference between the two groups. The

threshold value automatically induced from k-means classifier achieves 100% detection accuracy. Moreover, the possible range of threshold value for 100% detection accuracy is quite large, which facilitates practical selection of the threshold value and improves the robustness of the PCM method. T-test also reveals a significant difference in PCM detection results between pairs of nodes with or without direct causal relation with $p < 6.2397e - 25$ in all possible directions of the network. All these results provide effective methods in selecting the threshold value robustly in practice.

Q4. How long is the time series used in the numerical experiments?

A4. If not specified in the context of the corresponding experiments, all the simulations utilize 1000 time length series (with the sampling rate 1 Hz, so that the length matches exactly the time unit of the system).

Q5. How to guarantee the robustness of the numerical experiments?

A5. For all the examples of toy models, randomly selected are the 100 trials with a certain time length (usually 1000 time points if not specified) from 5000-length time series (here, the sampling rate is 1 Hz, so that the length matches exactly the time unit of the system). The average is calculated over results on these randomly selected trials. All the results are verified by the multi-testing corrections via the Bonferroni adjustment ($p < \alpha/n$), where n is the number of the edges in a network.

Q6. What are the numerical configurations and software packages used in the comparison studies?

A6. For the GC evaluations, we perform a standard GC test (i.e., F-test) and set the critical value of the significance (i.e., p -value) as 0.05. For consistency, we show the value $(0.05 - p)$ in the figures of relevance to represent the GC test results. We estimate and test the cGC and the pGC by using the MVGC Multivariate GC Toolbox v1.0 [17] and show in the figures of relevance the product of the index value and the significance value (i.e., 1 or 0). For the data from the toy model, we use the criterion, the AIC, to determine the model order with a ceiling value 10 time units when the GC, the cGC, the pGC are taken into account. However, for real-world data set, we determine the model order by AIC with the ceiling orders as, respectively, 5 time units for the DREAM4 GRN example, 60 time units for the air pollution with cardiovascular diseases system, 15 time units for the real gene regulatory network example, and 25 time units for the EEG example (the corresponding time units are stated in the text of each example). We normalize (i.e., detrend and demean) the time series when the GC method and its extensions are used in causations detection. For the TE evaluations, we utilize the package, TIM Matlab 1.2.0 (<http://www.cs.tut.fi/timhome/tim/tim.htm>). The evaluation procedure actually begins with the reconstruction of the state space also using the delay-coordinate embedding technique, which is the same as the phase reconstruction step in the PCM framework. The package uses 20 nearest neighbors and the mutual information to determine the value of the model lag (see the user documentation http://www.cs.tut.fi/timhome/tim/user_documentation.htm for details). The maximal lags are determined as 1, 10, 15, and 60 time units, respectively, for the logistic model, the plankton system, the real gene regulatory networks, and the air pollution with cardiovascular diseases system. Additionally, we use the permutation test to distinguish the causal link whose significance (p -value) is smaller than 0.05. The configurations of the pTE evaluations are in the almost same manner as those of the TE evaluations where only the estimator is changed to the partial version. For the case where the number of variables is more than three, we take each third-party variable as conditioning node and count the average pTE in the final results.

Q7. How to directly reproduce the numerical experiments in this research?

A7. We provided the references and access to all the data sets that we used in the research, and we also provide the codes for our PCM framework (publicly available at <https://github.com/Partial-Cross-Mapping>). Thus, using all these resources, one can reproduce all the results obtained in this work.

Supplementary Note 6. Additional information for real-world systems in the main text

6.1. Gene regulatory networks

In addition to the gene regulatory network shown in Fig. 4a of the main text, we investigate four other such networks, with structures shown in Supplementary Figure 12. Supplementary Figure 13 shows the detection accu-

racies versus the threshold T using both the PCM and MCM methods for the five gene regulatory networks. The ROC curves shown in the main text together with Supplementary Figure 13 demonstrate that the PCM method is remarkably effective in ascertaining direct causal links in gene regulatory networks.

6.2. Food chain of plankton species

In this analysis, the species abundances time series are measured from 12/07/1990 to 20/10/1997 with unequal sampling interval time. We interpolate the data to make equally-spaced time series with 794 points (the time unit of one time point is per 3.35 days). Supplementary Table 5 lists the p -values associated with all possible causal directions in the food chain network of three plankton species described in the main text. For all the direct links, the p -values are extremely small, signifying high statistical significance.

6.3. Air pollution and cardiovascular disease

Air pollution is believed to be one of the major causes of cardiovascular diseases. To establish this causal relation, we investigate real data sets of air pollutants and disease occurrence in the city of Hong Kong, where the collected data constitute the daily concentrations (in μgm^{-3}) of nitrogen dioxide (NO_2), sulfur dioxide (SO_2), respirable suspended particulate (Rsp_{ar}), and ozone (O_3) from the air-monitoring stations in Hong Kong from 1994 to 1997. Simultaneously recorded was the daily number of cardiovascular disease admissions (Cardio) into major hospitals in Hong Kong. To avoid the effect of sudden addition of hospital beds in early 1995, we choose the time series of 1000 days from March 1995 to November 1997 (the unit of one time point is per day). The corresponding p -values for all the possible causal directions with the PCM method are listed in Supplementary Table 6. Here, the significance index verified by the multi-testing corrections is set to be $p < 10^{-9}$.

Supplementary Note 7. Additional real-world examples: From gene regulatory networks to electrical information pathways

In order to further demonstrate the broad applicability of the PCM method, we investigate more real-world examples, revealing new viewpoints to the dynamical underpinnings of the real-world systems.

7.1. Reconstructing gene regulatory networks of circadian rhythm

We validate the effectiveness of our method with the real gene expression data. We consider the gene expression time series that were measured by Affimetrix microarray (Genechip Rat Genome 230 2.0) of the laboratory rat (*Rattus norvegicus*) cultured cells sampled from suprachiasmatic nucleus (SCN) for studying circadian rhythm [18, 19, 20, 21]. To elucidate the gene regulatory network architecture, we select the time series consisting of 16 time points, which is measured after the drug perturbation in the 19th hour (one measured time point corresponds to per 4.5 hours, more detailed information on data collection can be found in [18]). For the mammalian circadian clocks, it has been identified that there are approximately 17 genes involved in the core regulatory network, where the transcriptional circuits are formed by regulation of E/E' boxes, $DBP/E4BP4$ binding elements, and $RevErbA/ROR$ binding elements, respectively [22, 23]. Moreover, in addition to the gene-level interactions, there are also regulatory interactions at the protein level, e.g., the transcription factor *Clock* is phosphorylated by *PFK* family genes and the cytochrome genes, *Cry1* and *Cry2*, are phosphorylated by *MAPK* family genes [18]. Thus, we consider a gene regulatory network containing 17 core circadian genes and 20 kinase genes, as shown in Supplementary Figure 14(a). We interpolate the original time series to the series of 136 points (one point per half-hour). We thus apply the PCM method to the interpolated series to detect the directional regulatory relations among all the genes and depict the corresponding ROC curve in Supplementary Figure 14(b). As a comparison, we show the ROC curves obtained by using all the other causations detection methods in Supplementary Figure 14(b) as well.

We emphasize that the inference of the gene regulatory network based only on one single and short-term series is a challenging task. The existing inference methods can usually reach a value of AUC around 0.7 for synthetic data but only around 0.5 for real experimental data [24]. This is also confirmed by our comparison study. In

fact, for the 37-genes network, the GC-based and the TE-based methods can hardly detect any structure in the regulatory networks where the value of AUC is around 0.5, while the PCM method, whose AUC value reaches 0.65, outperforms all the other methods. In a relatively large network with very dense interactions, the current PCM method also could produce false negative detection results due to the over conditioning. Some optimal technique needs to be introduced to avoid such over conditioning situation, which becomes one of our present research works.

Additionally, we further demonstrate the effectiveness of the PCM method by investigating another sub-functional regulatory network with 18 genes, the core circadian genes and the *PFK* family [see Supplementary Figure 14(c)]. Clearly, the PCM method achieves a relatively high AUC value, approximately 0.73, while all the other methods cannot produce such a good performance in causations detection.

7.2. Revealing direct electrical information pathways in the human brain through EEG dataset

This example investigates the brain dynamics through analyzing the EEG recordings, which contain time series from 10 subjects with 19 electrodes per subject at a sampling rate of 256 Hz. Each recording lasts around 1 minute. All the data and their detailed descriptions are available at: <http://clopinnet.com/causality/data/nolte/> [1]. The data are filtered with a stop-band at 3 Hz to remove slow drifts. The data is divided into blocks of 4 seconds (i.e., 1024 data points) during which the recording is a continuous measurement that is cleaned of apparent artifacts. For each subject, we randomly select 10 blocks, calculate the PCM measures for every pair of electrode channels in the blocks, and show the average of the detection results in Supplementary Figure 15. Since the detection results on all the subjects show homogeneous properties, we further display an average over the detection results of all the subjects in Supplementary Figure 16(a). It shows that, instead of the remote connections between the brain regions, the signals (or information) are transferred majorly through the neighboring regions. This type of neighboring connections can be regarded as direct causations detected by our PCM framework. The detected connections also reveal the direct information pathways in the human brain. For example, the left hemisphere and the right hemisphere are connected successively by the middle channels, and a directional pathway is identified from frontal to dorsal channels in Supplementary Figure 16(a). These are consistent almost with the results presented in the literature [1, 15]. However, as shown in Supplementary Figure 16(b), using the MCM method in the same manner on the EEG data produces dense connections which are replete with indirect and remote links. This thus cannot bring any information pathways in the human brain.

Supplementary References

- [1] Nolte, G. *et al.* Robustly estimating the flow direction of information in complex physical systems. *Phys. Rev. Lett.* **100**, 234101 (2008).
- [2] Milo, R. *et al.* Network motifs: simple building blocks of complex networks. *Science* **298**, 824–827 (2002).
- [3] Alon, U. Network motifs: theory and experimental approaches. *Nat. Rev. Genet.* **8**, 450 (2007).
- [4] Noble, W. S. How does multiple testing correction work? *Nat. Biotechnol.* **27**, 1135 (2009).
- [5] Shaffer, J. P. Multiple hypothesis testing. *Annu. Rev. Psychol.* **46**, 561–584 (1995).
- [6] Barnett, L., Barrett, A. B. & Seth, A. K. Granger causality and transfer entropy are equivalent for gaussian variables. *Phys. Rev. Lett.* **103**, 238701 (2009).
- [7] Ma, H. *et al.* Detection of time delays and directional interactions based on time series from complex dynamical systems. *Phys. Rev. E* **96**, 012221 (2017).
- [8] Milojevic, A. *et al.* Short-term effects of air pollution on a range of cardiovascular events in england and wales: case-crossover analysis of the minap database, hospital admissions and mortality. *Heart* **100**, 1093–1098 (2014).
- [9] Duggento, A., Stankovski, T., McClintock, P. V. & Stefanovska, A. Dynamical bayesian inference of time-evolving interactions: From a pair of coupled oscillators to networks of oscillators. *Phys. Rev. E* **86**, 061126 (2012).
- [10] Stankovski, T., Duggento, A., McClintock, P. V. & Stefanovska, A. A tutorial on time-evolving dynamical bayesian inference. *Eur. Phys. J-Spec. Top.* **223**, 2685–2703 (2014).
- [11] Stankovski, T., Ticcinielli, V., McClintock, P. V. & Stefanovska, A. Coupling functions in networks of oscillators. *New J. Phys.* **17**, 035002 (2015).
- [12] Stankovski, T., Pereira, T., McClintock, P. V. & Stefanovska, A. Coupling functions: universal insights into dynamical interaction mechanisms. *Rev. Mod. Phys.* **89**, 045001 (2017).
- [13] Park, H.-J. & Friston, K. Structural and functional brain networks: from connections to cognition. *Science* **342**, 1238411 (2013).
- [14] Kantz, H. & Schreiber, T. *Nonlinear Time Series Analysis*, vol. 7 (Cambridge Univ. Press, Cambridge, 2004).
- [15] Harnack, D., Laminski, E., Schünemann, M. & Pawelzik, K. R. Topological causality in dynamical systems. *Phys. Rev. Lett.* **119**, 098301 (2017).
- [16] Hartigan, J. A. & Wong, M. A. Algorithm as 136: A k-means clustering algorithm. *J. R. Stat. Soc. C-Appl.* **28**, 100–108 (1979).
- [17] Barnett, L. & Seth, A. K. The mvgc multivariate granger causality toolbox: a new approach to granger-causal inference. *J. Neurosci. Meth.* **223**, 50–68 (2014).
- [18] Wang, Y., Zhang, X.-S. & Chen, L. A network biology study on circadian rhythm by integrating various omics data. *OMICS* **13**, 313–324 (2009).
- [19] Kawaguchi, S. *et al.* Establishment of cell lines derived from the rat suprachiasmatic nucleus. *Biochem. Bioph. Res. Co.* **355**, 555–561 (2007).
- [20] Morioka, R. *et al.* Phase shifts of circadian transcripts in rat suprachiasmatic nucleus. In *The Second International Symposium on Optimization and Systems Biology* (Citeseer, Pennsylvania, 2008).
- [21] Ma, H., Aihara, K. & Chen, L. Detecting causality from nonlinear dynamics with short-term time series. *Sci. Rep.* **4**, 7464 (2014).

- [22] Ueda, H. R. *et al.* System-level identification of transcriptional circuits underlying mammalian circadian clocks. *Nat. Genet.* **37**, 187 (2005).
- [23] Ko, C. H. & Takahashi, J. S. Molecular components of the mammalian circadian clock. *Hum. Mol. Genet.* **15**, R271–R277 (2006).
- [24] Wang, M. *et al.* Legumegrn: a gene regulatory network prediction server for functional and comparative studies. *PLoS One* **8**, e67434 (2013).